NORCE Norwegian Research Centre AS
www.norceresearch.no

Forskningsmidlene
for jordbruk og matindustri

End report

Detection of lameness and mastitis pathogens in milk using visual and olfactory sensing

Boyan Yuan[1], Håvard Nørstebø[2], Anne Catherine Whilst[2], and Nabil Belbachir[1]

[1]NORCE Norwegian Research Centre AS, [2]TINE SA

Report Norce Technology, 2020

October 20, 2020

Contents

List of Figures

Abstract

The objective of this project is to investigate feasibility of visual combined with olfactory sensing and multi-modal collaborative intelligence for the perception of diseases, especially the contagious ones, among a population of dairy cattle. The idea is to develop artificially intelligent systems that can generate low-dimensional representations about presence of diseases by learning from visual and olfactory sensory inputs, which are high-dimensional and noisy. The idea of in-cooperating visual and olfactory intelligence is a brilliant one; this is because the olfactory intelligence of animals and insects are predominant over visual intelligence and that olfactory intelligence are currently barely decoded computationally, i.e, no computational models outperform the olfactory perceptional capability of moths being widely studied. This is because in contrast to high-resolution camera sensors reaching many mega pixels, state-of-the-art volatile organic compounds sensing arrays called electronic nose achieve only tens of pixels and can only sense ppm maybe ppb concentration level (1 000 000 to 1 000 times lower than insects). The invention of multi-layer and large artificial neural networks for attempting to encode of human visual perceptual intelligence in a computational manner has achieved breakthrough in high-performance artificial intelligence systems. Newer models often contain one or more architectural modules which encodes cognitive science findings such as memory, contrast, analogy, anticipation of consequences, reasoning, knowledge in physics. We are targeting the derivation of a heterogeneous deep architecture combining the visual and olfactory branches their collaborative intelligence.

The scope of this project is to evaluate the potential of the proposed approach in a real world setup and to clarify technical challenges. Two specific scenarios are targeted:

- Digital dermatitis (DD). DD is a highly contagious disease and causes severe pain and lameness. The visual features of DD could be arched back, dropped neck and head owing to reduced strength in weight bearing by the infected foot. These are detected via 3D RGB-D (Red Green Blue - Depth) imaging. Another visual feature is the abnormal gait patterns of the in- fected foot owing to reduced locomotive abilities. These can be detected via gait analysis in videos.

- Mastitis. Mastitis is a bacterial inflammation in udders. It is relatively frequently occur-ing, highly contagious and causes pain, reduced milk production and low-quality milk. The visual features of mastitis could be elevated temperatures in infected region of udders. This can be detected by infrared thermography. Another visual feature could be abnormal smells owing to elevated concentrations of emitted volatile organic compounds owing to bacterial microbiological processes. This can be detected by electronic nose (or VOC gas sensors).

Detection of DD was investigated via extraction of geometric features of arched back as well as dropped neck and head of cattle suffering pain. A commercial low-cost 3D imager (RGB-D) imager (Intel Realsense D435) and its SDK (Software Development Kit) is used for **3D RGB-D imaging for 3D perception** while cattle are standing in the milking robot. 3D models of cattle's back and neck are obtained via converting of point cloud to mesh in software Meshlab. Within the limited sample set of cattle, although variations in arched angels in back and neck were found, no cattle showed signs of lameness, which was consistent with the ground truth. **Gait and behavior analysis** of these cattle in the panorama images and videos collected were hindered owing to that occlusions and that the activities of the animals are very limited (most of time they are standing or lying). **Activity recognition** in cattle was studied using a internet scraped image data of cattle in heat (estrous cycles) via deep convolution neural network model. Our conclusion is that by combining of 3D RGB-D based shape analysis, combined with gait and behavior analysis in videos, automatically and accurately assessment of DD is technically and practically feasible with the benefit of requiring only few low-cost visual sensors for monitoring of multiple even a large group of animals.

Detection of mastitis was investigated using a **thermal imaging camera** (Flir tau2, spectral band: 7.5 13.5μm, sensitivity: $<60mK$), the spatial and temporal variations in temperature of udder area of cattle while they are getting milked in milking robot were investigated. Within the limited sample set, obvious individual variations in mean temperatures and their standard deviations were

shown. Ground truth of whether one of more of the cattle had mastitis infection was not accurately identified, it was with high-confidence from laboratory analysis that no cattle had mastitis during the data collection period. The conclusion is that passive infrared thermography definitely could provide useful data for extraction of information about the health of udders and cattle harmlessly and low-costly (Only 1 sensor is needed). Variations in lighting condition and differences in shape and size of udder and the standing positions of cattles were found to provide considerable artifacts and noise to the recorded thermograms. Activity of cow is considered to influence overall temperature but not their spatial distributions. The problem of reconstruction of an approximately true model of the object, i.e., mastitis-presented udder and healthy udder via measurement data and prior knowledge such as the forward operator could be solved via inverse problem methods. Machine learning techniques come into play by constructing a model architecture with parameters being learned from data. We provide theoretical considerations in solving the non-linear inverse problem with unknown operator. The development of the theoretical and algorithmic framework will generate a wide range of applications within passive sensing such as acoustic emission and and passive infrared thermography for various applications.

Detection of mastitis was also studied by **artificial olfaction**. VOCs operating remotely or in the ambient without the need for guiding gas through a chamber such as in tunable diode laser absorption spectroscopy. The sensing of odorants using a traditional laboratory **gas chromatography - mass spectroscopy (GC-MS)** of 24 milk samples (15 infected and 9 healthy controls) for the purpose of identifying volatile organic compounds (VOC) biomarkers for mastitis infected milk were carried out. However, owing to accidental unknown bacteria development during the storage and transport of the samples contributed from dairy farms. The GC-MS results become more complicated. On the other hand, the existence of unique VOC biomarkers has been confirmed through a doctoral research carried out by Hettinga, et al., at Wageningen University in the Netherlands and others [5, 3, 4, 10, 6, 8, 3, 15, 13]. These studies showed that mastitis milk infected by bacterial - streptococcus aureus, coagulase-negative staphylococci, streptococcus uberis, streptococcus dysgalatiae, escherichia coli has a much higher overall concentrations in VOCs and several VOCs are identified as unique biomarkers for mastitis. These biomarkers are 2,3-butadione, Ethyl acetate, 2-methylbutanal, 2-pentanane, Isopentanol, Acetoin, Ethyl butyrate and few others. We know that VOCs are high-dimensional data, their patterns both in diversity (which VOCs) and concentrations can be complicated by a number of conditions. The identification of unique biomarkers shall be globally true, invariant to individual differences and variations in conditions affecting their generation. The discovery of a reliable biomarker in itself a research topic which is out of the scope of this project. We carried out **hyperspectral imaging Fourier transform infrared spectroscopy** for the detection of VOCs emitted by fungi causes degradation. This experiment showed that a key barrier in successful detection of VOCs are that their concentrations are extremely low (ppt to ppb). Such extremely low concentrations of molecules are beyond the detection limit of available gas sensors (Normally ppm some down to ppb range). Chemoresistive nanosensor arrays using sensing elements made of nanowires, nanotubes and graphenemay may mimic biological nose to detect more sensitively VOC molecules via changing their electrical resistance. The number of nanosensing elements can never go close to the number of olfactory receptors of human, dogs and insects. A **photo ionization detector (PID)** type gas sensor with detection limit of 1 ppb is planned to be tested in laboratory where the PID sensor is exposed to the head space of mastitis infected milk and healthy controls. The PID sensor can only detect overall VOC concentration levels not be able to know which VOCs are present. One of the electronic noses which has been widely used for artificial olfactory research is called Cyranose. Cyranose contains 32 nanocomposite sensing elements. Testing of Cyranose for mastitis detection has been considered.

A test-purpose state of the art sensors and data acquisition system was configured, and real-life data collection trials were carried out at the center for animal research (Ås Gård SHF). Machine learning algorithms was tested for early detection of lameness and mastitis.

- 3D RGB-D imaging
  3D models of the back of the cattle were obtained, although individual differences were detected, among the cattle analyzed no cattle showed features of abnormal shape of her back. This is consistent with the ground truth.

Feature detection algorithm based on ORB (Oriented FAST (Features for Accelerated Segment Test) and Rotated BRIEF(Binary Robust Independent Elementary Features)) was used for detecting keypoints of lam and healthy cattle. Keypoints of healthy cattle forms a straight line while those of lam cattle formed a broken and curved line.

- Activity recognition
  A pre-trained (on MS COCO dataset) deep convolution neural network model called faster R-CNN with Inception Resnet was retrained and used for heat detection. This model was benchmarked as the most accurate model among common mainstream models [11].

- Infrared thermography
  Infrared thermograms of 25 cattle were collected. Preliminary analysis of mean temperature and their standard deviations were used to classify homogeneous and non-homogenous udder skin temperature distributions. Solving non-linear inverse problem with unknown forward operators were studied at a theoretical level and implementation of computational code needing more resources will be conducted in a main project.

- GC-MS
  28 milk samples were analyzed with GC-MS at NMBU. Heat map of VOCs are generated. Dimensionablity reduction via principle component analysis using singular value decomposition projected the 24 data samples on a 2D plane of 2 principle components. These samples are segmented as 5 clusters. GC-MS based VOCs analysis can accurately classify milk samples but this method needs sample preparation and cannot be integrated in process. We did not find the same VOC biomarkers as reported in the literature; we doubt the milk samples were degraded during storage and produce artifacts in data. We think the detection of total VOC concentrations by low cost PID sensors could provide a promising qualitative screening tool.

Furthermore, we have evaluated **Hyperspectral imaging (short wavelength infrared and visual near infrared)**analysis of milk in powder form after removing water for detection of mastitis causing pathogens such as Escherichia coli (E. coli), Streptococcus uberis and Staphylococcus aureus. A **bioradar** sensor for respiratory pattern monitoring is also considered to provide useful information. These cannot be conducted within this project.

Results from this project will be published in relevant journals (Inverse problem in passive infrared thermography to Inverse problem journal in preparation or Neurips (Neuro information process- ing)workshop inverse problem meets deep learning) and conferences (Activity recognition to interna- tional conference of computer vision and pattern recognition (CVPR), Learning in spherical data to CVPR, or Neurips workshop deep learning through information geometry). A main research project was submitted to NFR's biotek program in 2018 and resubmitted to NFR's Fripro program in 2020. A resubmission to Landbruksdirektoratet in 2021 is planned.

Abstract

Målet med dette prosjektet er å undersøke muligheten for visuell kombinasjon med olfaktorisk sensing og multimodal intelligens for oppfatningen av sykdommer, spesielt de smittsomme, blant melkekyr. Ideen er å utvikle kunstig intelligens systemer som kan generere lavdimensjonale representasjoner om tilstedeværelse av sykdommer ved å lære av visuelle og olfaktoriske signal, som er høydimensjonale og støyende. Ideen om samarbeidende visuell og olfaktorisk intelligens er banebrytende. Dette er fordi luktintelligensen hos dyr og insekter er dominerende i forhold til visuell intelligens, og at kognitiv prosessen forbindet med luktintelligens for øyeblikket knapt dekodes algoritmisk. Dette er i motsetning til høyoppløselige kamerasensorer som når mange megapiksler, de beste sensor for å måle flyktige organiske gasser (VOC) som kalles elektronisk nese, bare oppnår titalls piksler og bare kan kjenne ppm, kanskje ppb konsentrasjonsnivå (1 000 000 til 1000 ganger lavere enn insekter). Oppfinnelsen av flerlags og store kunstige nevrale nettverk for å forsøke å kode menneskelig visuell perseptuell intelligens på en algoritmisk måte har oppnådd et gjennombrudd i høyytelses kunstige intelligenssystemer. Nyere modeller inneholder ofte en eller flere arkitektoniske moduler som koder for kognitive vitenskapelige funn som minne, kontrast, analogi, forventning om konsekvenser, kausalitet, kunnskap i fysikk. Vi retter oss mot avledningen av en heterogen, dyp arkitektur som kombinerer de visuelle og olfaktoriske grenene deres samarbeidene intelligens.

Omfanget av dette prosjektet er å evaluere potensialet i den foreslåtte tilnærmingen i et reelt verdensoppsett og å avklare tekniske utfordringer. To spesifikke scenarier er målrettet:

- Digital dermatitt(DD). DD er en svært smittsom sykdom og forårsaker alvorlig smerte og halthet. De visuelle egenskapene til DD kan være buet rygg, tapt nakke og hode på grunn av redusert styrke i vektbæring av den infiserte foten. Disse blir oppdaget via 3D RGB-D (Rød Grønn Blå -Dybde) bildebehandling. Et annet visuelt egenskapet er unormale gangmønstre for den infiserte foten på grunn av reduserte lokomotivevner. Disse kan oppdages via ganganalyse i videoer.

- Mastitt. Mastitt er en bakteriell betennelse i jur. Det forekommer relativt ofte, er veldig smittsomt og forårsaker smerte, redusert melkeproduksjon og melk av lav kvalitet. De visuelle egenskapene til mastitt kan være forhøyede temperaturer i infisert område av jur. Dette kan oppdages ved infrarød termografi. Et annet visuelt egenskapet kan være unormal lukt på grunn av forhøyede konsentrasjoner av utslipp av VOC på grunn av bakterielle mikrobiologiske prosesser. Dette kan oppdages med elektronisk nese (eller VOC gas sensorer).

Påvisning av DD ble undersøkt ved ekstraksjon av geometriske properti ved buet rygg, også nakke-og hodehode som lider av smerte. En kommersiell lavkostnad 3D-kamera (RGB-D)(Intel Realsense D435) og dens SDK (Software Development Kit) brukes til **3D RGB-D bildebehandling for 3D-oppfatning** mens kyr står i melkeroboten. 3D-modeller av kyrs rygg og nakke oppnås ved å konvertere punktsky til mesh i programvaren Meshlab. Innenfor det begrensede prøvesettet med kyr, selv om det ble funnet variasjoner i buede grader i rygg og nakke, viste ingen kyr tegn på halthet, noe som var i samsvar med sannheten. **Gang- og atferdsanalyse** av disse kyr i panoramabildene og videoene som ble samlet inn ble hindret på grunn av at okklusjoner og at aktivitetene til dyrene er svært begrenset (mesteparten av tiden de står eller ligger). **Aktivitetsgjenkjenning** hos kyr ble studert ved hjelp av skrapte bildedata på internett av kyr i heat (estrous sykluser) via dyp konvolusjon nevrale nettverksmodell. Konklusjonen vår er at ved å kombinere 3D RGB-D-basert bildeanalyse, kombinert med gang- og atferdsanalyse i videoer, automatisk og nøyaktig vurdering av DD er teknisk og praktisk gjennomførbar med fordelen av å kreve bare noen få billige visuelle sensorer for overvåking av flere til og med en stor gruppe dyr.

Deteksjon av mastitt ble undersøkt ved hjelp av et **termisk kamera** (Flir tau2, spektralbånd: 7, 5 − 13, 5 *mum*, følsomhet: < 60*mK*), de romlige og tidsmessige variasjonene i temperaturen på jurområdet hos kyr mens de blir melket i melkrobot ble det undersøkt. Innenfor det begrensede prøvesettet ble tydelige individuelle variasjoner i gjennomsnittstemperaturer og deres standardavvik vist. Sannhet om hvorvidt et av flere av kyr hadde mastittinfeksjon, ble ikke identifisert nøyaktig, det var med høy tillit fra laboratorieanalyse at ingen kyr hadde mastitt i løpet av datainnsamlingsperioden.

Konklusjonen er at passiv infrarød termografi definitivt kan gi nyttige data for utvinning av informasjon om helsen til jur og kyr ufarlig og billig (bare 1 sensor er nødvendig). Variasjoner i lysforhold og forskjeller i form og størrelse på juret og stående stillinger til kyr ble funnet å gi betydelige gjenstander og støy til de registrerte termogrammene. Aktivitet av ku anses å påvirke den totale temperaturen, men ikke deres romlige fordeling. Problemet med rekonstruksjon av en tilnærmet sann modell av objektet, dvs. mastitt-presentert jur og sunn jur via måledata og forkunnskaper som den fremre operatøren, kan løses via inverse problemmetoder. Maskinlæringsteknikker spiller inn ved å konstruere en modellarkitektur med parametere som læres av data. Vi gir teoretiske betraktninger for å løse det ikke-lineære inverse problemet med ukjent operatør. Utviklingen av det teoretiske og algoritmiske rammeverket vil generere et bredt spekter av applikasjoner innen passiv sensing som akustisk utslipp og og passiv infrarød termografi for forskjellige applikasjoner.

Påvisning av mastitt ble også studert av **kunstig olfaksjon**. VOC som opererer eksternt eller i omgivelsene uten behov for å lede gass gjennom et kammer, for eksempel i avstemmelig diode-laserabsorpsjonsspektroskopi. Oppdagelsen av luktsto˙er ved bruk av et tradisjonelt laboratorium **gasskromatografi - massespektroskopi (GC-MS)** av 24 melkeprøver (15 infiserte og 9 sunne kon-troller) for å identifisere biomarkører for VOC for mastittinfisert melk ble utført. På grunn av utilsiktet ukjent bakterieutvikling under lagring og transport av prøvene bidro imidlertid fra melkeproduksjon. GC-MS-resultatene blir mer kompliserte. På den annen side har eksistensen av unike VOC-biomarkører blitt bekreftet gjennom en doktorgradsundersøkelse utført av Hettinga et al. Ved Wageningen University i Nederland og andre [5, 3, 4, 10, 6, 8, 3, 15, 13]. Disse studiene viste at mastittemelk infisert av bakterie - streptococcus aureus, koagulase-negative stafylokokker, streptococcus uberis, streptococcus dysgalatiae, escherichia coli har en mye høyere total konsentrasjon i VOC, og flere VOC er identifisert som unike biomarkører for mastitt. Disse biomarkørene er 2,3-butadion, etylacetat, 2-metylbutanal, 2-pentanan, isopentanol, acetino, etylbutyrat og få andre. Vi forstår at VOC er høydimensjonale data, deres mønstre både i mangfold (hvilke VOC) og konsentrasjoner kan kompliseres av en rekke forhold. Identifikasjonen av unike biomarkører skal være globalt sant, uforanderlig i forhold til individuelle forskjeller og variasjoner i forhold som påvirker deres generasjon. Oppdagelsen av en pålitelig biomarkør i seg selv et forskningstema som er utenfor omfanget av dette prosjektet. Vi utførte **hyperspektral avbildning Fourier transform infrarød spektroskopi** for påvisning av VOC som sendes ut av sopp forårsaker nedbrytning. Dette eksperimentet viste at en viktig barriere i vellykket deteksjon av VOC er at konsentrasjonen er ekstremt lav (ppt til ppb). Slike ekstremt lave konsentrasjoner av molekyler er utenfor deteksjonsgrensen for tilgjengelige gassensorer (normalt ppm noen ned til ppb-området). Kjemoresistive nanosensorarrays som bruker sensingelementer laget av nanotråder, nanorør og grafen, kan etterligne biologisk nese for å oppdage mer følsom VOC-molekyler ved å endre deres elektriske motstand. Antallet nanosensingelementer kan aldri komme i nærheten av antall luktreseptorer fra mennesker, hunder og insekter. En **foto-ioniseringsdetektor (PID)** type gassføler med deteksjonsgrense på 1 ppb er planlagt å bli testet i laboratorium der PID-sensoren blir utsatt for headspace til mastittinfisert melk og sunne kontroller. PID-sensoren kan bare oppdage samlede VOC-konsentrasjonsnivåer, og kan ikke vite hvilke VOCer som er tilstede. En av de elektroniske nesene som har blitt mye brukt til kunstig olfaktorisk forskning kalles Cyranose. Cyranose inneholder 32 nanokompositt sensingelementer. Testing av Cyranose for påvisning av mastitt har blitt vurdert.

En advansert sensorer og datainnsamlingssystem ble konfigurert, og virkelige datainnsamlingsforsøk ble utført ved senter for dyreforskning (Ås Gård SHF). Maskinlæringsalgoritmer ble testet for tidlig påvisning av halthet og mastitt.

- 3D RGB-D avbildning
  3D-modeller av baksiden av kyr ble oppnådd, selv om det ble oppdaget individuelle forskjeller, blant kyr som ble analysert, viste ingen kyr funksjoner med unormal form på ryggen. Dette er i samsvar med sannheten.
  Funksjonsdetekteringsalgoritme basert på ORB (Oriented FAST (Features for Accelerated Seg-ment Test) og Rotated BRIEF (Binary Robust Independent Elementary Features)) ble brukt til å oppdage kritiske punkter fra lam og sunt kyr. Mønsteren for sunne kyr danner en rett linje mens lam av kyr dannet en avbrudd og uregelmessig linje.
- Aktivitetsgjenkjenning

En pre-trent (på MS COCO datasett) dyp konvolusjon nevrale nettverksmodell kalt raskere R-CNN med Inception Resnet ble omskolert og brukt til heat deteksjon. Denne modellen ble vurdert som den mest nøyaktige modellen blant vanlige modeller [11].

- Infrarød termografi
  Det ble samlet inn infrarøde termogrammer på 25 kyr. Foreløpige analyser av gjennomsnittstemperatur og deres standardavvik ble brukt til å klassifisere homogene og ikke-homogene fordeler på jurhudtemperatur. Å løse ikke-lineære inverse problemer med ukjente fremoveroperatører ble studert på et teoretisk nivå, og implementering av beregningskode som trenger flere ressurser vil bli utført i et hovedprosjekt.

- GC-MS
  28 melkeprøver ble analysert med GC-MS ved NMBU. Varmekart over VOC genereres. Dimensjonsreduksjonsreduksjon via prinsippkomponentanalyse ved bruk av singular verdi-dekomponering projiserte de 24 datasamplene på et 2D-plan med 2 hovedkomponenter. Disse prøvene er segmentert som 5 klynger. GC-MS-basert VOC-analyse kan klassifisere melkeprøver nøyaktig, men denne metoden trenger forberedelse av prøven og kan ikke integreres i prosessen. Vi fant ikke de samme VOC-biomarkørene som rapportert i litteraturen; vi tviler på at melkeprøvene ble nedbrutt under lagring og produserer gjenstander i data. Vi tror deteksjonen av totale VOC-konsentrasjoner av lave PID-sensorer kan gi et lovende kvalitativt screeningverktøy.

Videre har vi evaluert **Hyperspectral imaging (kort bølgelengde infrarød og visuell nær infrarød)** analyse av melk i pulverform etter fjerning av vann for påvisning av mastitt som forårsaker patogener som Escherichia coli (E. coli), Streptococcus uberis og Staphylococcus aureus . En **bioradar** -sensor for åndedrettsmønsterovervåking anses også å gi nyttig informasjon. Disse kan ikke gjennomføres innenfor dette prosjektet.

Resultatene fra dette prosjektet vil bli publisert i relevante tidsskrifter (Invers problem i passiv infrarød termografi til Inverse problem journal under forberedelse eller Neurips (Neuro informasjonsbehandling) workshop invers problem møter dyp læring) og konferanser (Aktivitetsgjenkjenning til internasjonal konferanse om datasyn og mønster anerkjennelse (CVPR), Læring i sfæriske data til CVPR, eller Neurips workshop dyp læring gjennom informasjonsgeometri). Et hovedforskningsprosjekt ble levert til NFRs biotek-program i 2018 og sendt inn på nytt til NFRs Fripro-program i 2020. Det er planlagt en nyinnlevering til FFL/JA forskingsmidler i 2021.

Acknowledgements

Financial support from the Agriculture and Food Industry Research Funds(FFL/JA) is greatly appreciated. We thank Professor Judith Narvhus and Senior Engineer Kari Olsen at NMBU for their assistance in GC-MS analysis.

Chapter 1

Introduction

Breakout of contagious diseases such as mastitis owing to bacterial inflammation in udder, digital dermatitis (DD) causing lameness, BRSV (Bovine Respiratory Syncytial Virus, causing cough), BCoV (Bovine Corona Virus, causing diarrhea) virus infections, causes significant economic losses. Lameness caused by DD or other infections, which is a contagious and extremely painful, is one of the most significant welfare and productivity issues livestock farming. These causes direct economic losses of hundreds of millions NOK every year. In addition, use of antibiotics in livestock and antibiotic resistance imposes health risks to human consumers. Today for prevention of some of the diseases, such as Mastitis and lameness no effective vaccines are available; neither are there low-cost and non-invasive methods available for safe and effective screening. Alternative methods of using wearable sensors and lab on a chip, which usually measures value of a single physical parameter, are either non-effective or very costly.

Today, the public actions in fighting against breakout of contagious diseases have been concentrated on restricting contact and limit mobility of the animals, for example, to carry out blood tests when buying and selling the animals, and to require immediately reporting when one sick case is suspected, to confine the scope of spreading. These defensive actions have been effective; however, it is a reactive action and its detection is dependent on the observations of the farmers. It is not proactive, thus, not effective in disease prevention. This is evidenced by TINE who expressed their worries that diseases are extremely contagious and spreading rapidly also during the incubation period when no observations of sickness are possible. Neither can farmers timely isolate sick cattle when it gets sick during nighttime. As response to the urgent need of establishing technologies and methods to proactively fight again contagious diseases and for increasing productivity in general, TINE has initiated a Norwegian Agriculture DataCloud (Landbrukets Datasky) project. The basic idea is to collect available data from various sources and attempt to make use of the data through cloud computing. Real-time data are not available at the moment, but the Landbrukets Datasky project team are working on implementing real time data in order to possibly realize timely and early warning of risks of contagious diseases.

There are currently some measurements are integrated with milking robots such as chromatography, somatic bacterial counting, and measure volume and flow rate of milking. Those measurements are insufficient to detection mastitis timely. Value losses caused by mastitis infection increases drastically when mastitis is detected in bulk tank milk and in later stages, because this means a large volume milk has been contaminated.

The research community of Precision Livestock Farming have been focused on the development of either wearable sensors such as vital parameters sensors, or lab on a chip type of solution. So far, only GPS sensor based bells have been widely worn by relatively large animals. Other wearable sensors that normally need direct contact with the body of the animals can be easily destroyed. Lab on a chip solution is difficult to use, and can be too expensive for use on a regular basis. Machine vision and fusion of electronic tongue, electronic nose and vision have been investigated for forestry mapping, lameness monitoring and food safety research. However, they have not been investigated for early warning of risks of contagious diseases in livestock. At NORCE, we have researched the use of nanosensor array for olfactory perception of disease, and using various sensors for non-invasive detection of rot due to fungi in wood.

We proposed and investigated artificial sensory perception, i.e., 360° panorama imaging, 3D RGB-D imaging, infrared thermography and artificial olfactory (GC-MS) perceptions for DD and mastitis detection. 360° imaging camera was used for registration of images and videos data for extracting knowledge about abnormal appearance and activity patterns; 3D RGB-D imaging was utilized for generating 3D shape descriptors; infrared thermal camera for detection of abnormal skin temperature distributions; and nanosensor arrays for smelling bad odor (volatile organic compounds). The artificial sensory perception system utilized low-cost, non-contact, non-invasive sensors to provide continuous and real-time data for monitoring of single and multiple animals, and used artificial intelligence for perception for uncovering underlying diseases, thus provided an adequate and low-cost solution for avoiding economic losses.

The primary object of the project was to evaluate feasibility of the proposed artificial sensory perception concept for non-invasive and continuous monitoring of livestock to enable early warning of risk of contagious diseases, using detection of lameness and mastitis pathogens in milk as two cases.

The main objective was realized through the following 4 sub-objectives (SO).

Completed SO 1. Configured adequate visual and artificial olfactory sensing systems for lameness and mastitis pathogens detection via 3D RBG-D imaging, infrared thermal imaging, 360 °. imaging, and GC-MS analysis.

Completed SO 2. Collected videos and images of cattle and VOC data in milk at Ås farm SHF. Dataset: 3D RGB-D imaging of 23 cattle, infared thermograms of udder of 25 cattle, GC-MS data of 28 samples.

Completed SO 3. Algorithms for detection of lameness and mastitis pathogens in milk.

- Keypoints detection based on ORB algorithm for back shape descriptor extraction.
- 3D model construction using Meshlab toolbox.
- Fast RCNN with Inseption RESNET deep neural network model trained for activity recognition.
- Statistical analysis of infrared thermograms data for classification. Algorithms for solving inverse problem with unknown forward operator such as based Bayesian inversion and combining deep generative models are considered theoretically.
- Principle component analysis was used for dimensionality reduction and clustering of GC-MS data.

Completed SO 4. Evaluated feasibility visual and olfactory sensing system in detection of lameness and mastitis pathogens in milk.

Visual and olfactory sensing system showed interesting results. Given the continued dedication in collecting and managing the database and constructing high-performance machine learning models either via domain expertise and/or with automated model searching pipeline, these artificially intelligent systems will with no doubt be an independent tool for future precision livestock farming. We point out that VOC sensing down to concentration level of ppb to ppt is a challenging task, however nano electronic nose are under rapid development. Combing with neuro-morphic computing chip and neural computing engine, real-time processing and inferences without the need of storage of large amount of data enables real-world deployment of these systems.

Chapter 2

Data collection

Dataset is a most important infrastructure for building machine learning models for learning a low-dimensional representation in high-dimensional data. A good rule of thumb is that the number of samples need to be roughly 10 times the number of Vapnik–Chervonenkis (VC) dimensions of the model. This means millions of data for normal size deep neural nets. Indeed, it is not only about the absolute number of samples but also their distributions. Redundant data deteriorates training performance. To enable good generalization of the model, the distribution of training data and distribution of testing data needs to be similar. To create a large scale and high quality dataset is not a trivial task. Many open datasets find with labeled training data for the machine learning and artificial intelligence community to use freely. One example is the activity recognition task dataset. Data are well chosen, consistent, and usually in a format easy to load such as .csv or .png. However, this is not the case for industrial applications where data is rather limited. An emerging learning concept called few shot and one shot learning is interesting for limited data. Currently, error rate of few short learning algorithms are considerably high.

A dataset using a panoramaic lens, a depth imager, an infrared thermal camera was collected at the Åsgård farm in December 2018. GC-MS dataset was obtained in September 2019. A statistical overview of the dataset shall be provided, however, given the limited scope, this does not make sense at the pre-project phase.

Data such as milked volume and flow speed for each cattle with their identification number are available as additional data. Currently these data are not used. Figure [**milk_robot_data**] shows examples of the milk volume data.

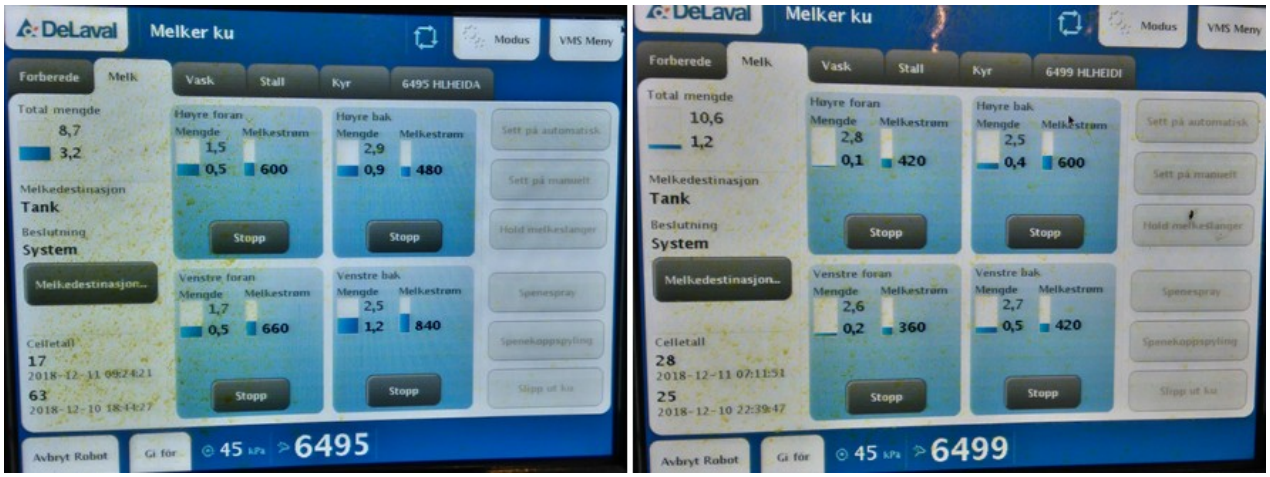

Figure 2.1: Milk volume data collected in milk robot.

2.1 3D RGB-D dataset

RGB-D data is streamed as a video and stored as a .bag file which was converted to .ply and .png files. Depth data in csv format was extracted using intel realsense SDK rs-convert. This imaging setup enables the reconstruction of back and neck 3D model of the cattle. Figure 2.2 shows the intel realsense RGBD camera. 2.3 shows an example of RGBD images.

Figure 2.2: RGB-D(depth)for 3D model reconstruction of back and neck of the cattle while getting milked in the milking robot.

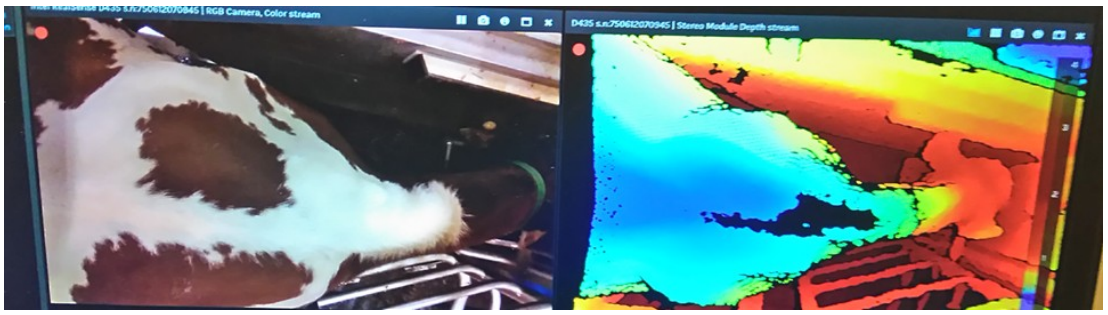

Figure 2.3: An exmaple of RGBD images.

2.2 360° panorama dataset

Figure 2.4 shows the 360° panorama camera mounted at the roof railing at the Ås farm for video streaming. 360-degree panorama camera enables wide field-of-view imaging using a single lens, but at the cost of distortions. The distortions cause failure in object recognition task when using convolution kernels normally used for perspective images. Methods for learning in hemispherical and spherical data is summarized in previous work part.

2.3 Long wavelength infrared thermography dataset

Passive infrared thermal camera can be used to image temperature field of a scene. By choosing a camera with a high spatial resolution (a large number of pixels) and a high sensitivity (how small difference in temperature is distinguishable), a dense and precise temperature field can be obtained. Heterogeneity in temperature field could indicate heterogeneity in thermal conductivity and capacity of the medium giving no ambient inputs such as lighting or other thermal convection which attributes to the local discontinuity in temperature fields. By transferring the data into frequency domain via discrete Fourier transform, certain features are revealed. Figure 2.6 shows the long wavelength infrared thermal camera for udder surface temperature field imaging while the cattle get milked in the milking robot. 2.7 shows an example of infrared thermal camera image.

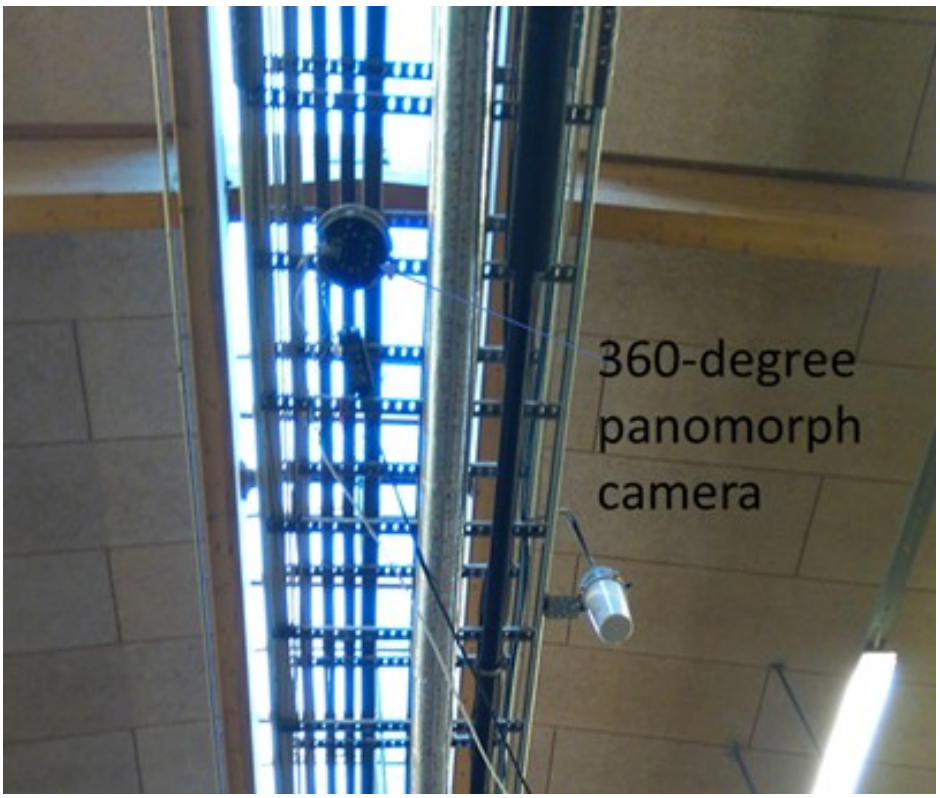

Figure 2.4: 360-degree panorama camera for video streaming.

Figure 2.5: An example of 360° panorama images.

2.4 GC-MS dataset

The purpose of using laboratory gas chromatography - mass spectroscopy for the profiling of volatile organic compound contents in milk samples (both mastitis pathogen infected milk and healthy controls) is to identify distinct biomarkers that distinguishing the two groups. Essentially, this means dimensionality reduction in feature space. When considering olfactory perception of human or dogs, the basic idea is to identify the odorants that give the distinct smell when milk gets spoiled or when milk comes from a sick cow. An important question needs to be answered is that how low concentrations of odorants can be sniffed by dogs comparing to how low concentrations is detected by a GC-MS

Figure 2.6: Long wavelength infrared thermal camera for udder surface temperature field imaging while the cattle get milked in the milking robot.

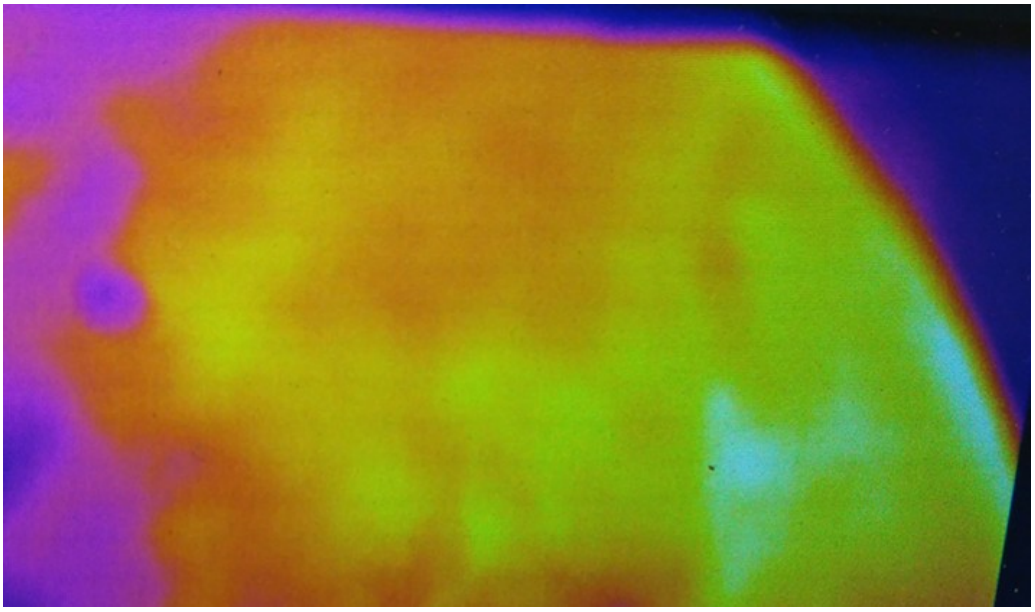

Figure 2.7: An example of infrared thermal camera image.

spectroscopy. Olfactory receptor of dogs can detect odorants at concentrations at low as 1-2 parts per trillion (ppt), which is 10,000-100,000 times more sensitive than human, and is 1,000,000 times more sensitive than a normal GC-MS with detection limit of 1 ppm. This is the main bottleneck that LAS (laser absorption spectroscopy), GCMS, FTIR (Fourier transform infrared spectroscopy) are not able to achieve sniffing out disease while dogs even human can. Emerging nanosensing elements such as using metal oxide semiconductor (MOS) nanowire, carbon nanotubes, graphene, nanocantilever holds promise to achieve lower detection limit, research remains at the laboratory.

For electronic nose, commercially available electronic nose devices find many. We have investigated PEN3 and cyranose for headspace gas analysis. The term “headspace” is referred as the gas directly surrounding a sample. The constituents of the sample which have a high volatility will generally be present in the headspace in higher concentrations. Low volatile compounds are less likely to be found in a sample. Consequently, the concentration of molecules present in the headspace is not proportional to the concentration of the same molecules in liquid or solid sample. PEN3 is one that appeared in

several research papers. There are 10 MOS in PEN3, all different types and heated up at specific temperatures (350°C - 500°C) in order to catch the widest range of volatile compounds. Cost is 19800 Euro. MOS are calibrated in-house with reference gas standards; by experience I can honestly say there is very little drifting over time and lifetime of sensors is several years, depending on how it is operated by users. It gets rid of humidity by automatically heating up the measuring chamber at 110°C. PEN3 is a complex electronic nose for fingerprinting and recognition that is worldwidely known for being one of the leaders in the sector.

PEN3 is an analytical instrument which basically consists of a combination of an array of 10 different metal oxide sensors and pattern recognition software. The electronic nose is capable to recognize simple or complex mixtures of organic vapors after an appropriate training period. The results are determined through statistical methods like euclid, correlation, factor analysis (PCA) or discriminant function analysis (DFA). The system can be used for fast quality control applications in the food and chemical industry. Environmental and safety applications are also possible.

The detection limit of the PEN3 is in the range of 1ppm. Sensors with good selectivity for sulfur organic compounds, methane, hydrogen, alcohol and hydrocarbons are used.

The analytical system has a special sampling system integrated, which by an automatic control (autoranging) prevents an overloading of the sensors and also leads to a better and faster qualitative and quantitative. The system is easy to handle. We recommend only a short training.

You can use the PEN as a standalone device without pre-treatment of gas streams or together with a headspace sampler or with our Trap and thermal Devices (EDU) to enhance the selectivity of the sample.

Chapter 3

Data analysis for mastitis and digital dermatitis detection

3.1 Theoretical framework and state-of-the-art

3.1.1 360° vision

Convolutinal neural networks (CNNs) for spherical data The main challenge of convolutional operation in spherical data is that rotation non-equivalence. When sliding the convolutional filters across a perspective image, this operation is translational. However, for hemispherical or spherical data, the imaging domain is non-Euclidean, the convolution involves rotation of 3D orthogonal group, SO(3). Coors et al.[17] presented a novel convolutional kernel which is invariant to latitudinal distortions via projection of a regular sampling pattern to its tangent plane. Similarly, Su et al.[14] proposed an adaptive CNN kernels applied to the equirectangular projection of sphere, i.e., the CNN kernels are alike the ones for the locally projected patches.

Cohen et al.[16] presented a novel way treating convolution on spherical data as a three dimensional manifold, i.e., special orthogonal group (SO(3)) and using generalized Fourier transform for fast group correlation. Subsequently, Esteves et al.[18] modeled 3D data with multi-valued spherical functions and proposed a novel spherical convolutional network that implements exact convolutions on the sphere by realizing them in the spherical harmonic domain. Yu et al.[24] pointed out that spherical CNN loses the object's location and overlarge bandwidth is required to preserve a small object's information on a sphere. And they proposed a novel grid-based spherical CNN (G-SCNN) which transforms a spherical image to a conformal grid map to be the input to the S2/SO3 convolution. Defferrard et al. and Perraudin et al. [21, 22] presented a graph based spherical CNN named DeepSphere. Their idea is to model the sampled sphere as a graph of connected pixels and using the length of the shortest path between two pixels as an approximation of the geodesic distance between them. Yang et al. [29]generalized the grid-based CNNs to a non-Euclidean space by taking into account the geometry of spherical surfaces and propose a Spherical Graph Convolutional Network (SGCN) to encode rotation equivariant representations.

Tens of new models are proposed for visual understanding in spherical data recently. Zhao et al. [30] proposed a 360° detector named Reprojection R-CNN by combining the advantages of both ERP and PSP, which generates spherical bounding boxes. The method was evaluated on a synthetic dataset for detection of salient objects like person and train. Wang et al. [23] used a modified RCNN model for object detection in synthesized dataset 360GoogleStreetView. Chou et al. [25] a real-world 360° panorama dataset containing common objects of 37 categories. Lee et al. [27] proposed to project spherical images onto an icosahedral spherical polyhedron and apply convolution on transformed images. Figure 2.4 shows a panorama camera using the panorama lens of Immervision mounted at the roof railing at Ås farm. 2.5 shows an example of dewarped panorama image. Figure 3.13 shows a research done on the detection of lameness via detection of small change in shape of back and neck.

3.1.2 Non-linear dimensionality reduction via manifold learning

We utilize a multi-modal sensory approach for collaboratively detection of a underlying early stage disease. We consider firstly knowledge generation from each of the uni-modal sensing methods individually. The focus are on methods which can be applied to different sensing modalities such as 3D depth imaging data, panorama vision, infrared thermograms and GC-M data. These methods include dimensionality reduction via concepts such as subspace and union of subspaces (UoS), manifold learning [19]. They model signal as low-dimensional subspace embedded in a high-dimensional ambient space. Two- and three-dimensional manifolds are components of geometrical model of the objects [2]. Learning theory development such as using reproducing kernel Hilbert space or Banach space as well as metric and manifold learning model learning of a model from examples essentially the learning of relationships (including distances) between observations.

Riemannian manifold learning (RML)has been proposed for nonlinear dimensionality reduction (NLDR)[1]. A Riemannian manifold can be constructed in the form of a simplicial complex, and thus its intrinsic dimension can be reliably estimated. Then the NLDR problem is solved by constructing Riemannian normal coordinates (RNC). The method can learn the data's intrinsic geometric structure, yielding uniformly distributed and well organized low-dimensional embedding data.

Riemannian metric is a concept of distance expressed by means of a smooth positive definite symmetric bilinear form defined on the tangent space at each point. Distance functions and loss functions play important roles in machine learning to obtain good models. Similar to learning in Hilbert space vs. Banach space, Riemannian geometry generalize Euclidean geometry. The notion of a directional derivative of a function from multivariable calculus is extended in Riemannian geometry to the notion of a covariant derivative of a tensor. Many concepts and techniques of analysis and differential equations have been generalized to the setting of Riemannian manifolds. A distance- preserving diffeomorphism between Riemannian manifolds is called an isometry. This notion can also be defined locally, i.e. for small neighborhoods of points. Any two regular curves are locally isometric. However, the existence of a local isometry imposes strong compatibility conditions on their metrics: the Gaussian curvatures at the corresponding points must be the same. In higher dimensions, the Riemann curvature tensor is an important pointwise invariant associated with a Riemannian manifold that measures how close it is to being flat. An important class of Riemannian manifolds is the Riemannian symmetric spaces, whose curvature is not necessarily constant. These are the closest analogues to the "ordinary" plane and space considered in Euclidean and non-Euclidean geometry. Pseudo-Riemannian geometry generalizes Riemannian geometry to the case in which the metric tensor need not be positive-definite. Finsler manifolds is a generalization of Remannian manifolds.

Perrault et al. [9] studied algorithms for preserving original geometry (such as distances, angles, areas, volume, etc) of the data after performing non-linear dimension reduction. The approach is based on augmenting the output of an embedding algorithm with geometric information embodied in the Riemannian metric of the manifold. The Riemannian metric allows one to compute geometric quantities (such as angle, length, or volume) for any coordinate system or embedding of the manifold. Figure 3.1 shows the transformation of data in Euclidean space to non-Euclidean manifold space while keeping isometries.

3.1.3 Artificial olfaction

The nanosensor array microsystem shall have more pixels such as 100 (10 x 10 array). This nanoarray SoC (system on chip) can be integrated with micro hotplate and on-chip automatic calibration. It is adequate for profiling complex mixtures of odours containing hundreds of volatile organic compounds (VOCs) at concentrations down to ppb. Artificial intelligence algorithms, especially deep neural network models (DNNs) and algorithms are developed to de-mix odours and recognize a presenting diseaseous odour from the response patterns registered by the nanoarray. Both the nanoarray and DNN models and algorithms have not been investigated by the research community today and will be developed in this project to achieve breakthrough. Microarray analysis for gene expressions have gone from obscurity to being almost ubiquitous in biological research within few years, we trust that this is likely a case for the ubiquitous use of nanoarray for breath profiling and uncovering underlying health conditions. This is

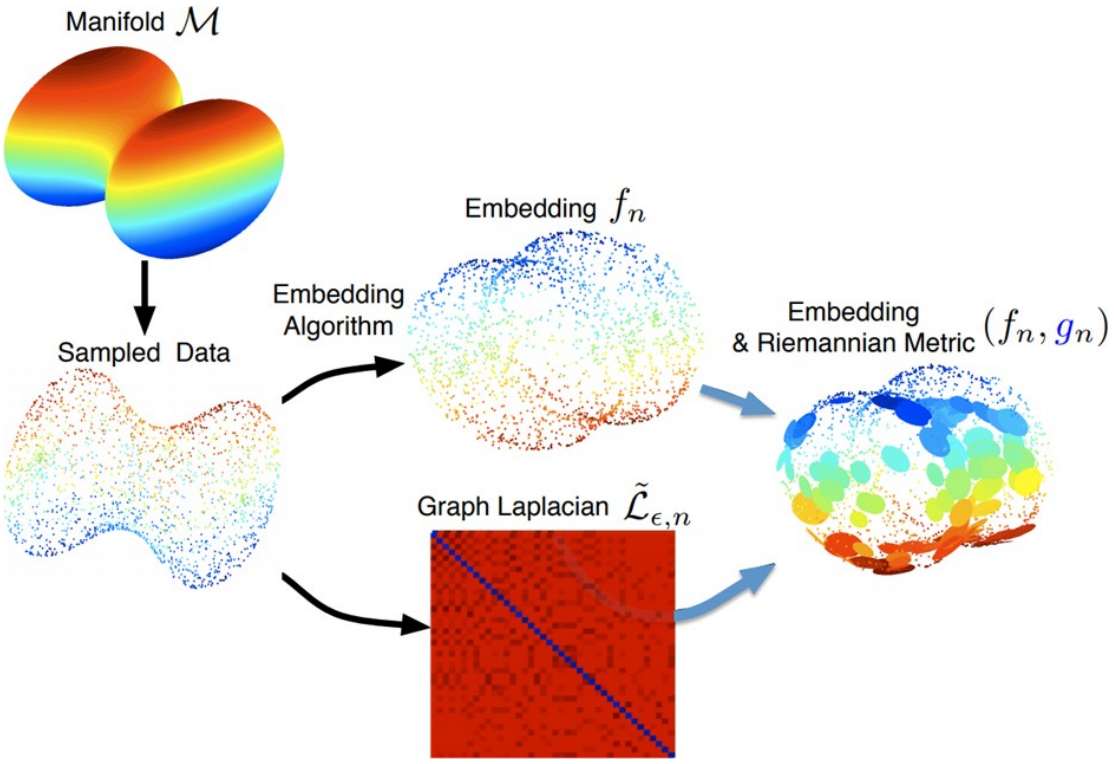

Figure 3.1: Metric learning and manifold in machine learning

because that, firstly, diagnostics based on VOC biomarkers provides a completely painless, non-invasive, and low-cost method with potential to be integrated with the sensing platform of a smart phone for everywhere and anytime health care. Secondly, it is, in nature, a highly-sensitive sensing modality, thus, enabling early-stage disease detection, which is deterministic in successful disease treatment. The high-sensitivity and early-stage detection advantage is rendered by the high-mobility, long-diffusion length and high permeability of gaseous particles, which contrasts with traditional biomarkers carried in cells, blood, urine and faeces. When comparing to otherwise modern diagnostic imaging methods such as X-ray computed tomography, Ultrasonic and Magnetic Resonance Imaging, which utilize reflected and scattered waves by an abnormality to reconstruct its image for diagnostics, although are extremely powerful and robust, often have difficulties in distinguishing early-stage diseaseous cells.

Disease and other diseases prediction through identification of VOC biomarkers in exhaled breath has been extensively investigated. Consensus findings on VOC biomarkers researcher are that a number of VOCs are associate with diseases or other diseases invariant to other subject characteristics; and that the association is rather deviations in concentrations of a small cluster of VOCs from normal ranges of concentrations rather than the presence or non-presence of a certain VOC or certain VOCs. The VOCs' concentration patterns are subject characteristics-invariant, and they solely depend on disease or non-disease . These studies are truly ground-breaking, especially remarkable are the pioneering research carried out by Professor Hossam Haick at Technion-Israel University of Technology. Gas Chromatography-Mass Spectroscopy is a benchmark analytical equipment for laboratory gas analysis. Gas sensing utilizing otherwise laser absorption spectroscopy such as Tuneable diode laser absorption spectroscopy (TDLAS) can also achieve very low detection limits (of the order of ppb), however, these techniques have limitations in detecting multiple gases simultaneously (even for TDLAS), therefore it finds limited use in breath analysis. Professor Charles M. Lieber at Harvard University made the first nanowire nanosensor using silicon nanowire and is leading silicon and MOS nanowires based MOSFET (MOS Field Emission Transistor) for future nanoelectronics. From a commercial maturity point of view, a number of companies in Europe and USA have commercialized nanosensors. These include Sensigent , Vista Therapeutics (Founded by Professor Charles M. Lieber at Harvard University), and NanosensorsTM. We studied a type of piezoresistive nanosensors made by NanosensorsTM.

Although ground-breaking research has been carried out by world-renowned groups, many challenges remain which hinders its application clinically. These include the intrinsic challenges with the chemo- resistive nanosensors such as humidity interferences, cross-reactivity, long-term drift, stability, and relatively short life-time. The latter shortcomings are because, simply speaking , the sensing materials changes their electrical resistivity through changing their carrier densities owing to adsorption and absorption of gas molecules; the adsorption and absorption processes are not 100% reversible, thus leaving a non-virgin sensing interface impairing sensitivity. These challenges, however, will be tackled in this research through on-board auto-calibration. Except for these challenges, in our viewpoint, the dimensions of the nanosensor array (21 sensors [12] or 14 sensors [7]) investigated in the state-of-the-art research [2-26] are insufficient for adequate sensing of VOCs in breath as a complex system. This is because that breath data are high-dimensional data. The breath samples are constituted of commonly 100-200 VOCs with various concentrations (The total VOCs of biological origin is about 1877), and they are dependent to the so-called subject characteristics such as age, gender, alcohol, smoke, drug, disease, geographical, location (why the person live), historical exposure of exogeneous VOCs, and other metabolic, pathological, and physiological processes associated parameters.

The insufficient dimensionality of nanoarrays is not likely owing to non-awareness but owing to technical difficulties in constructing such as high-dimension array. As to our best understanding, the bottleneck in hindering achieving a large nanoarray does not lie in the creation of nanostructures and nanomaterials, it is rather lie in a smart CMOS integration of sensing layer with circuitries such as signal conditioning, digital signal processing, auto-calibration, and temperature control of micro hotplate. Important issues also include low noise, input and output signal range, signal resolution, accuracy, and sampling rates . In this aspect, we see that the method used for manufacturing the gold nanoparticles nanosensor array by Professor Hossam Haick's group can be a reason that larger array at 32-pixels failed. CMOS integration of nanosensors for gas sensing both for silicon nanowire which can be made by top-down approach and other semiconductor nanowire made by bottom-up approach was studied. IBM has made large scale production of silicon nanowire transistors. Engineering design of CMOS interface electronics for nano-bio-sensor platform on nanometer CMOS technology have been studied. It is worth noting of a new development in CMOS integrated graphene as imaging sensors for multispectral and hyperspectral imaging could provide this research an approach in fabricating CMOS integrated 100-pixels nanoarray.

Our second opinion is that artificial intelligence, especially DNN models and algorithms, which have been produced ground-breaking results in visual perception and speech recognition, shall be developed for olfactory perception. In this aspect, current research front has been limited to traditional algorithms such as principle component analysis, linear discriminant analysis and discriminant factor analysis (DFA) binary classifiers, using only 4 data points from sensor response curves. In evaluating whether DNN models and algorithms are promising methods, we reviewed findings in neuroscience in understanding of mammal's olfactory intelligence and can perceive the common features between olfactory and visual intelligence. Thus, we will be focusing on developing new DNN models and algorithms for robust artificial olfactory perception. It is not impossible that novel DNN models could be constructed, giving a novel nanoarray data structure. Furthermore, hyperspectral sensor provides both spatial (providing structural/geometrical information) and spectral (providing chemical information) information, we think that algorithms developed for hyperspectral imaging can be useful for nanoarray.

A more recent work published in 2018 confirmed that 3-Methyl-butanoic acid was a stable end product and its production correlated well with the growth of Staph. aureus at different temperatures and in different mixtures with other pathogens (except Salmonella Enteritidis) in sterile milk.

3.1.4 Activity recognition in video

The detection of lameness in cow using computer vision has been researched. Figure 3.9 shows work done on gait analysis for detection of lameness in cattle. We did not carry out gait analysis within this project because TINE suggested us to focus on mastitis detection.

Table 4

Recent applications of electronic-nose technologies for the noninvasive early diagnosis of gastrointestinal diseases.

Disease [1]	Location	Sample	N =	E-Nose Model	Sensor Type/No. [2]	References
BAD	BAD	Urine	110	Fox 4000	MOS 18	[76]
Cancer	Colon	Breath	26	Experimental	GNP 14	[98]
	Colon	Fecal	157	Cyranose 320	CBPC 32	[5]
CRC/IBD	Colon	Urine	92	WOLF	EC 8, NDIR 2, PID 1	[2]
IBD	Intestine	Urine	62	Owlstone	FAIMS	[99,100]
	Colon	Fecal	83	Cyranose 320	CBPC 32	[101]
IBS	Colon	Fecal	182	Experimental	GC-MOS 1	[102]
	Colon	Breath	234	V&F Airsense	IMR-MS	[77]
ID	Colon	Fecal	100	Experimental	GC-MOS 1	[103]
LOS	Systemic	Fecal	76	Cyranose 320	CBPC 32	[95]
NEC	Colon	Fecal	27	Cyranose 320	CBPC 32	[104]

[1] Disease abbreviations: BAD = Bile acid diarrhea; CRC = Colorectal cancer; IBD = Inflammatory bowel disease; IBS = Irritable bowel syndrome; ID = Infectious diarrhea; LOS = Late-onset sepsis; NEC = Necrotizing enterocolitis.
[2] Sensor type abbreviations and number in sensor array: CBPC = carbon black polymer composite; EC = electrochemical sensor; FAIM = field asymmetric ion mobility spectroscopy; GC = gas chromatography; GNP = gold nanoparticles; IMR-MS = ion molecule reaction-mass spectrometry; IMS = ion mobility spectrometry; MOS = metal oxide semiconductor, NDIR = non-dispersive infra-red (optical devices); PID = photo-ionization detector.

Figure 3.2: Cyranose320 and other enoses including PID sensor.

Table 1. Quantity of volatile metabolites in the milk samples[1]

	Mastitis pathogen					
Metabolite	*Staph. aureus*	CNS	*Strep. uberis*	*Strep. dysgalactiae*	*E. coli*	Control[2]
Acetaldehyde	7.4×10^{6a}	6.4×10^{4b}	2.8×10^{5b}	1.4×10^{5ab}	2.7×10^{5ab}	1.2×10^{5b}
2,3-Butadione	1.1×10^{6a}	5.0×10^{4ab}	5.6×10^{5ab}	1.4×10^{5ab}	1.5×10^{4b}	0^{b}
2-Butanone	2.1×10^{6a}	3.2×10^{5b}	1.4×10^{6ab}	7.0×10^{5ab}	5.0×10^{5ab}	3.0×10^{6a}
Ethyl acetate	1.1×10^{6a}	0^{b}	5.0×10^{4b}	2.0×10^{4b}	6.9×10^{5a}	0^{b}
3-Methylbutanal	2.8×10^{7a}	2.7×10^{6a}	8.8×10^{4b}	4.5×10^{5b}	4.6×10^{4b}	6.4×10^{3b}
2-Methylbutanal	3.7×10^{5a}	5.9×10^{4a}	2.7×10^{3b}	2.7×10^{3b}	0^{b}	0^{b}
2-Pentanone	8.1×10^{4a}	8.3×10^{3b}	3.6×10^{4b}	7.1×10^{4ab}	9.6×10^{5ab}	0^{b}
Acetic acid	6.0×10^{6a}	5.1×10^{5b}	2.7×10^{6ab}	3.4×10^{6ab}	9.8×10^{6a}	3.7×10^{6ab}
Isopentanol	7.3×10^{6a}	1.1×10^{6ab}	0^{b}	1.3×10^{5b}	3.9×10^{6b}	0^{b}
Acetoin	8.2×10^{5a}	3.2×10^{3b}	3.6×10^{3b}	0^{b}	0^{b}	0^{b}
Ethyl butyrate	7.2×10^{5a}	0^{b}	7.2×10^{4b}	1.0×10^{5b}	3.3×10^{5ab}	0^{b}
Butyric acid	2.9×10^{6ab}	2.0×10^{5c}	7.8×10^{5c}	1.0×10^{6abc}	1.0×10^{6abc}	4.15×10^{6a}
Ethyl 2-methyl butyrate	2.2×10^{4a}	3.6×10^{2b}	0^{b}	0^{b}	0^{b}	0^{b}
Ethyl 3-methyl butyrate	9.6×10^{4a}	4.6×10^{2b}	3.2×10^{3b}	2.8×10^{3b}	0^{b}	0^{b}
3-Methyl butyrate	1.4×10^{2}	0	0	7.2×10^{2}	0	0
2-Methyl butyrate	6.0×10^{4}	0	0	0	0	0
2-Heptanone	1.7×10^{5a}	1.9×10^{4b}	1.0×10^{5ab}	1.3×10^{5ab}	3.2×10^{5ab}	2.0×10^{4b}
Butyl butyrate	1.2×10^{4a}	0^{b}	0^{b}	0^{b}	0^{b}	0^{b}
Ethyl hexanoate	3.7×10^{5a}	7.6×10^{2b}	6.4×10^{4b}	9.2×10^{4ab}	2.2×10^{5a}	0^{b}

[a–c]Means within a row with different superscripts differ ($P < 0.05$).
[1]Numbers are mean area values (arbitrary units) of the different volatiles of the samples that did contain the compounds of interest.
[2]Milk from cows without clinical mastitis and with low SCC.

Figure 3.3: VOC profiles obtained by GCMS analysis by Hettinga without Ethanol.

Table 4.1. Quantity of volatile metabolites in the milk samples. Numbers are mean area values (arbitrary units) of the different volatiles of the samples which did contain the components of interest.

Metabolite [1]	Mastitis Pathogen					Control [3]
	Staph. aureus	CNS [2]	*Strep. uberis*	*Strep. dysgalactiae*	*E. coli*	
Acetaldehyde	$7.4\times10^{6\,a}$	$6.4\times10^{4\,b}$	$2.8\times10^{5\,b}$	$1.4\times10^{5\,ab}$	$2.7\times10^{5\,ab}$	$1.2\times10^{5\,b}$
Ethanol	$1.1\times10^{8\,a}$	$1.6\times10^{5\,b}$	$1.6\times10^{6\,b}$	$5.8\times10^{6\,b}$	$1.3\times10^{8\,a}$	$0^{\,b}$
2,3-Butadione	$1.1\times10^{6\,a}$	$5.0\times10^{4\,ab}$	$5.6\times10^{5\,ab}$	$1.4\times10^{5\,ab}$	$1.5\times10^{4\,b}$	$0^{\,b}$
2-Butanone	$2.1\times10^{6\,a}$	$3.2\times10^{5\,b}$	$1.4\times10^{6\,ab}$	$7.0\times10^{5\,ab}$	$5.0\times10^{5\,ab}$	$3.0\times10^{6\,a}$
Eth. acetate	$1.1\times10^{6\,a}$	$0^{\,b}$	$5.0\times10^{4\,b}$	$2.0\times10^{4\,b}$	$6.9\times10^{5\,a}$	$0^{\,b}$
3-Meth.butanal	$2.8\times10^{7\,a}$	$2.7\times10^{6\,a}$	$8.8\times10^{4\,b}$	$4.5\times10^{5\,b}$	$4.6\times10^{4\,b}$	$6.4\times10^{3\,\,b}$
2-Meth.butanal	$3.7\times10^{5\,a}$	$5.9\times10^{4\,a}$	$2.7\times10^{3\,b}$	$2.7\times10^{3\,b}$	$0^{\,b}$	$0^{\,b}$
2-Pentanone	$8.1\times10^{4\,a}$	$8.3\times10^{3\,b}$	$3.6\times10^{4\,b}$	$7.1\times10^{4\,ab}$	$9.6\times10^{5\,ab}$	$0^{\,b}$
Acetic acid	$6.0\times10^{6\,a}$	$5.1\times10^{5\,b}$	$2.7\times10^{6\,ab}$	$3.4\times10^{6\,ab}$	$9.8\times10^{6\,a}$	$3.7\times10^{6\,ab}$
Isopentanol	$7.3\times10^{6\,a}$	$1.1\times10^{6\,ab}$	$0^{\,b}$	$1.3\times10^{5\,b}$	$3.9\times10^{6\,b}$	$0^{\,b}$
Acetoin	$8.2\times10^{5\,a}$	$3.2\times10^{3\,b}$	$3.6\times10^{3\,b}$	$0^{\,b}$	0 b	$0^{\,b}$
Eth. butyrate	$7.2\times10^{5\,a}$	$0^{\,b}$	$7.2\times10^{4\,b}$	$1.0\times10^{5\,b}$	$3.3\times10^{5\,ab}$	$0^{\,b}$
Butyric acid	$2.9\times10^{6\,ab}$	$2.0\times10^{5\,c}$	$7.8\times10^{5\,c}$	$1.0\times10^{6\,abc}$	$1.0\times10^{6\,abc}$	$4.2\times10^{6\,a}$
Eth. 2-meth.but.	$2.2\times10^{4\,a}$	$3.6\times10^{2\,b}$	$0^{\,b}$	$0^{\,b}$	$0^{\,b}$	$0^{\,b}$
Eth. 3-meth.but.	$9.6\times10^{4\,a}$	$4.6\times10^{2\,b}$	$3.2\times10^{3\,b}$	$2.8\times10^{3\,b}$	$0^{\,b}$	$0^{\,b}$
3-Meth.but.	1.4×10^{2}	0	0	7.2×10^{2}	0	0
2-Meth.but.	6.0×10^{4}	0	0	0	0	0
2-Heptanone	$1.7\times10^{5\,a}$	$1.9\times10^{4\,b}$	$1.0\times10^{5\,ab}$	$1.3\times10^{5\,ab}$	$3.2\times10^{5\,ab}$	$2.0\times10^{4\,b}$
Butyl but.	$1.2\times10^{4\,a}$	$0^{\,b}$	$0^{\,b}$	$0^{\,b}$	$0^{\,b}$	$0^{\,b}$
Eth. hexanoate	$3.7\times10^{5\,a}$	$7.6\times10^{2\,b}$	$6.4\times10^{4\,b}$	$9.2\times10^{4\,ab}$	$2.2\times10^{5\,a}$	$0^{\,b}$

[a, b, c] Means within a row with different superscripts differ ($P < 0.05$)

[1] Eth. = Ethyl; Meth. = Methyl; But. = Butyrate

[2] CNS = coagulase-negative staphylococci

[3] Milk from cows without clinical mastitis and with low somatic cell count

Figure 3.4: VOC profiles obtained by GCMS analysis by Hettinga with Ethanol.

3.1.5 Inverse problem in infrared thermography using a deep generative model as prior

Image processing such as reconstruction (computational imaging) as in compressive sensing, denoising, inpainting and machine learning can be cast into an inverse problem. On the other hand, deep generative models such as generative adversarial network can be learned using examples. The learned model can be used as prior in Bayesian inversion scheme [20]. Figure [**inv_dgm**] shows a general framework under development at NORCE Technology and Energy department.

Figure 3.11 shows a summary of a number of research been conducted on infrared thermography for the evaluation of udder health.

Figure 3.10 shows a workflow for solving inverse problem in active infrared thermography. The experimental data are collected in a set up for landmine detection using microwave induced thermal wave propagation. The forward process are governed by the Maxwell's electrodynamics equations coupled to the heat equation (Laplace equation), both are partial differential equations. The objective function of the inverse problem is formulated as a $l2$ norm, i,e., a non-linear least squares minimization problem. This minimization problem is solved by generic algorithm and pattern search algorithm. This is a clever approach for utilizing measured data most. However, for the case of passive infrared thermography, the underlying thermal imbalance and thermal diffusion process are unknown, neither are inputs from the ambient such as lighting conditions be defined accurately. In the problem formulation of inverse problem, this means that the transformation matrix (often denoted as A) which mapping the input (often denoted as x) into the output (often denoted as y)is unknown, in addition to that the input is unknown.

Table 2 Median concentrations of VOCs released or consumed by *Staphylococcus aureus*

Compound	CAS	m/z for SIM	median concentrations [ppbv]				
			medium	1.5 h	3.0 h	4.5 h	6.0 h
propanal	123-38-6	57	3.955	***10.62***	***14.22***	***8.932***	***7.04***
3-methyl-2-butenal	107-86-8	55, 84	1.526	1.832	***3.415***	***5.708***	***5.348***
2-ethylacrolein	922-63-4	84	1.656	2.01	***6.453***	***5.537***	***5.775***
(Z)-2-methyl-2-butenal	1115-11-3	84	73.48	81.91	***177.4***	***268.5***	***247.9***
(E)-2-methyl-2-butenal	497-03-0	84	< LOD	< LOD	***0.259***	***0.394***	***0.381***
benzaldehyde §	100-52-7	107	20.64	19.08	17.65	**12.66**	**3.815**
methacrolein	78-85-3	70	5.922	5.644	***9.328***	7.617	6.36
acetaldehyde	75-07-0	43	528.5	606.4	***374.2***	***1022.7***	***1417.4***
3-methylbutanal **	590-86-3	-	317.1	***403.3***	***2764.3***	***4779.3***	***4818.5***
2-methylpropanal **	78-84-2	-	598.6	658.5	***2044.5***	***1698.6***	***1299.5***
1-butanol	71-36-3	56	< LOD	< LOD	< LOD	***21.24***	***59.4***
2-methyl-1-propanol	78-83-1	56, 74	0	0	0	***21.32***	***52.62***
3-methyl-1-butanol	123-51-3	55, 70	0	0	0	***27.65***	***210.0***
ethanol **	64-17-5	-	0	***89.57***	***237.0***	***6173.0***	***11695.1***
acetoin (hydroxybutanone)	513-86-0	88	< LOD	***3.59***	***8.004***	***140.6***	***279.3***
acetol (hydroxyacetone)	116-09-6	74	< LOD	< LOD	< LOD	***113.5***	***331.0***
2,3-butanedione	431-03-8	86	22.65	23.92	27.45	***49.84***	***67.99***
acetic acid	64-19-7	45, 60	0	0	0	***880.5***	***2566.6***
isovaleric acid	503-74-2	60	0	0	0	***31.13***	***97.35***
ethyl acetate	141-78-6	61	0	0	0	***1.973***	***5.624***
n-butyl acetate	123-86-4	56, 73	0	0	0	***0***	***0.239***
ethyl isovalerate	108-64-5	70	0	0	0	< LOD	***0.852***
isopentyl acetate	123-92-2	55, 70	0	0	0	< LOD	***1.938***
ethyl formate	109-94-4	31	0	0	0	< LOD	***3.188***
methyl methacrylate **	80-62-6	-	15.99	14.79	20.27	***28.65***	***31.93***
methanethiol	74-93-1	47	134.2	***210.4***	***360.6***	***559.4***	***701.5***
dimethyldisulfide (DMDS)	624-92-0	94	1.558	2.221	***3.657***	***8.134***	***10.24***
1,3-butadiene	106-99-0	54	< LOD	< LOD	***4.941***	***4.342***	***4.313***
2-methylpropene	115-11-7	56	< LOD	< LOD	***4.546***	***14.31***	***21.89***
n-butane	106-97-8	58	0.664	0.703	***1.274***	***2.504***	***4.329***
(Z)-2-butene	590-18-1	56	0	0	< LOD	***3.687***	***4.789***
(E)-2-butene	624-64-6	56	1.344	< LOD	***4.793***	***11.32***	***13.73***
propane	74-98-6	43, 41	0.91	0.815	1.951	***3.441***	***4.902***

Bold numbers indicate significant difference (Kruskal-Wallis test) in VOC concentrations between bacteria cultures and medium headspace ($p < 0.05$). Ethanol, 2-methylpropanal, 3- methylbutanal and methyl methacrylate were analyzed in TIC mode as indicated by **, while the remaining compounds were analyzed in

Figure 3.5: VOC profiles obtained by GCMS analysis by Philipiak with Ethanol as the main VOC.

3.2 Results and discussion

3.2.1 3D RGB-D

The depth data is calibrated and 3D model of the back and neck of the cattle is reconstructed. RGB-D 3D perception has important applications within mobile robots and autonomous vehicles for 3D simultaneous localization, mapping and navigation. Super-resolution 3D imaging in certain applications combined with a Lidar sensor provides possibility for small change detection such as the case of arched back and neck when cattle suffering pain. 3D convolution kernels is an extension of 2D kernels and can be constructed in tensorflow, pytorch or keras without much difficulty.

Figures 3.14 and 3.15 shows the 3D model obtained from RGBD imaging of four cows. Algorithms for feature detection and and description include speeded up robust features (SURF)),

scale-invariant feature transformer (SIFT), FAST, BRIEF and ORB. SURF is a scale- and rotation- invariant detector and descriptor. They are usually implemented on gray-scale images. SURF uses an integer approximation of the determinant of Hessian blob detector, which can be computed with 3 integer operations using a precomputed integral image. Its feature descriptor is based on the sum of the Haar wavelet response around the point of interest. These can also be computed with the aid of the integral image. ORB is an efficient alternative to SIFT and SURF. Opencv has easy interfaces for implementing feature detection and description algorithms by calling the class and running functions such as create(), detect(), compute(). As shown in 3.16 and 3.17, a direct implementation of the feature

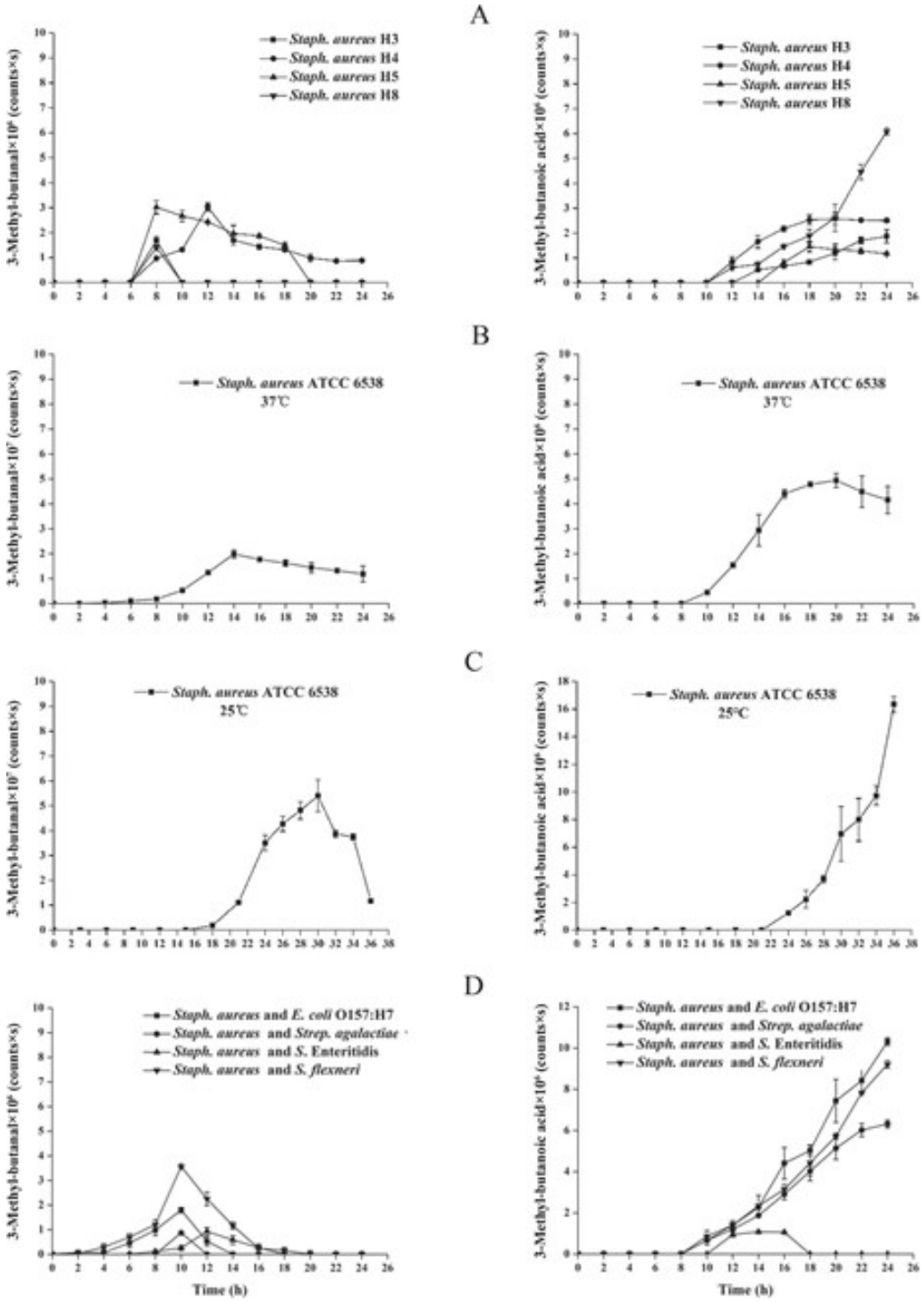

Figure 3.6: The 2018 result showed that 3-Methyl-butanoic acid is a good biomarker.

detector and descriptor algorithms cannot produce satisfactory results.

By focusing on the back region via simply cropping the images, as shown in Figure 3.18 classification of lameness and healthy status are transformed into distinguishing the shape connecting the keypoints detected. The keypoints of healthy cow makes a straight line while that of the lameness makes a broken and non-straight lines.

Shape descriptors extraction could result in interesting feature vectors for classification of lameness and healthy cows.

The openPose library provide methods for real-time multi-person to jointly detect human body,

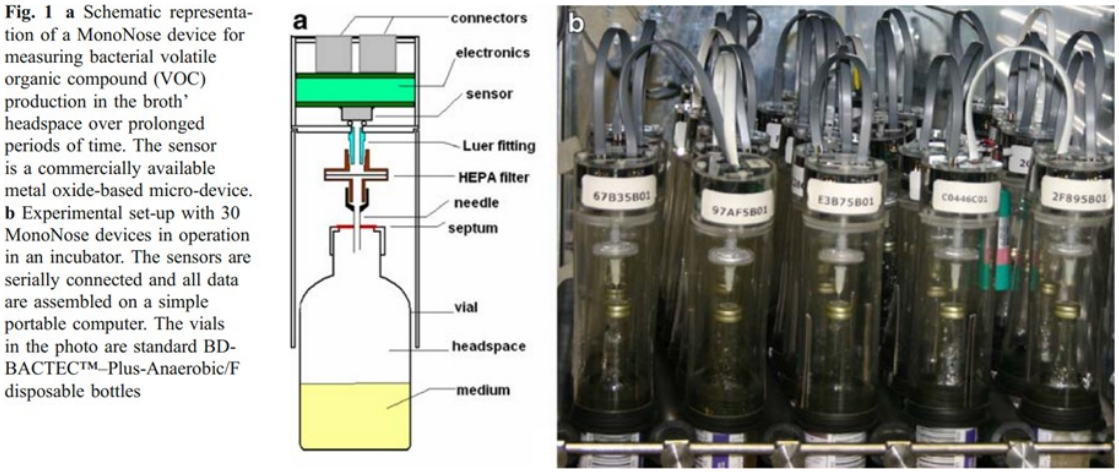

Fig. 1 **a** Schematic representation of a MonoNose device for measuring bacterial volatile organic compound (VOC) production in the broth' headspace over prolonged periods of time. The sensor is a commercially available metal oxide-based micro-device. **b** Experimental set-up with 30 MonoNose devices in operation in an incubator. The sensors are serially connected and all data are assembled on a simple portable computer. The vials in the photo are standard BD-BACTEC™–Plus-Anaerobic/F disposable bottles

Figure 3.7: VOC analysis using a single type commercial MOS gas sensor.

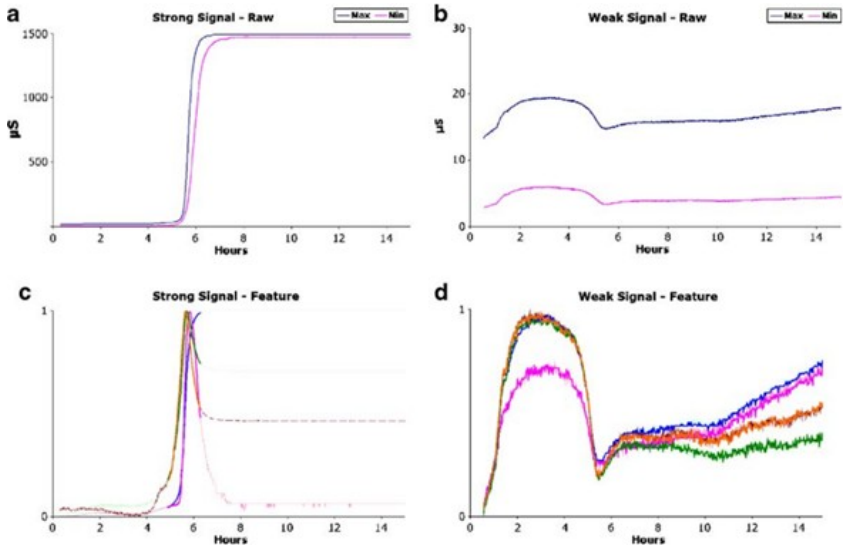

Figure 3.8: Results of VOC analysis using a single type commercial MOS gas sensor.

Figure 3.9: Lameness detection using gait analysis.

hand, facial, and foot keypoints (in total 135 keypoints) on single images. Most of the pose and gait analysis algorithms and toolboxes are designed for human. Because cows body geometrical arrangement, kinematics and dynamics are different from human, adaptions are needed. To obtain robust detection, the algorithms need to distinguish normal individual variations such as normal variations in geometrical shape of lame cow and healthy cow. The robustness and accuracy can be improved by comparing not only differences in these features between different individuals but also the same individuals at different time period such as when lame and when healthy. An important factor to consider is that

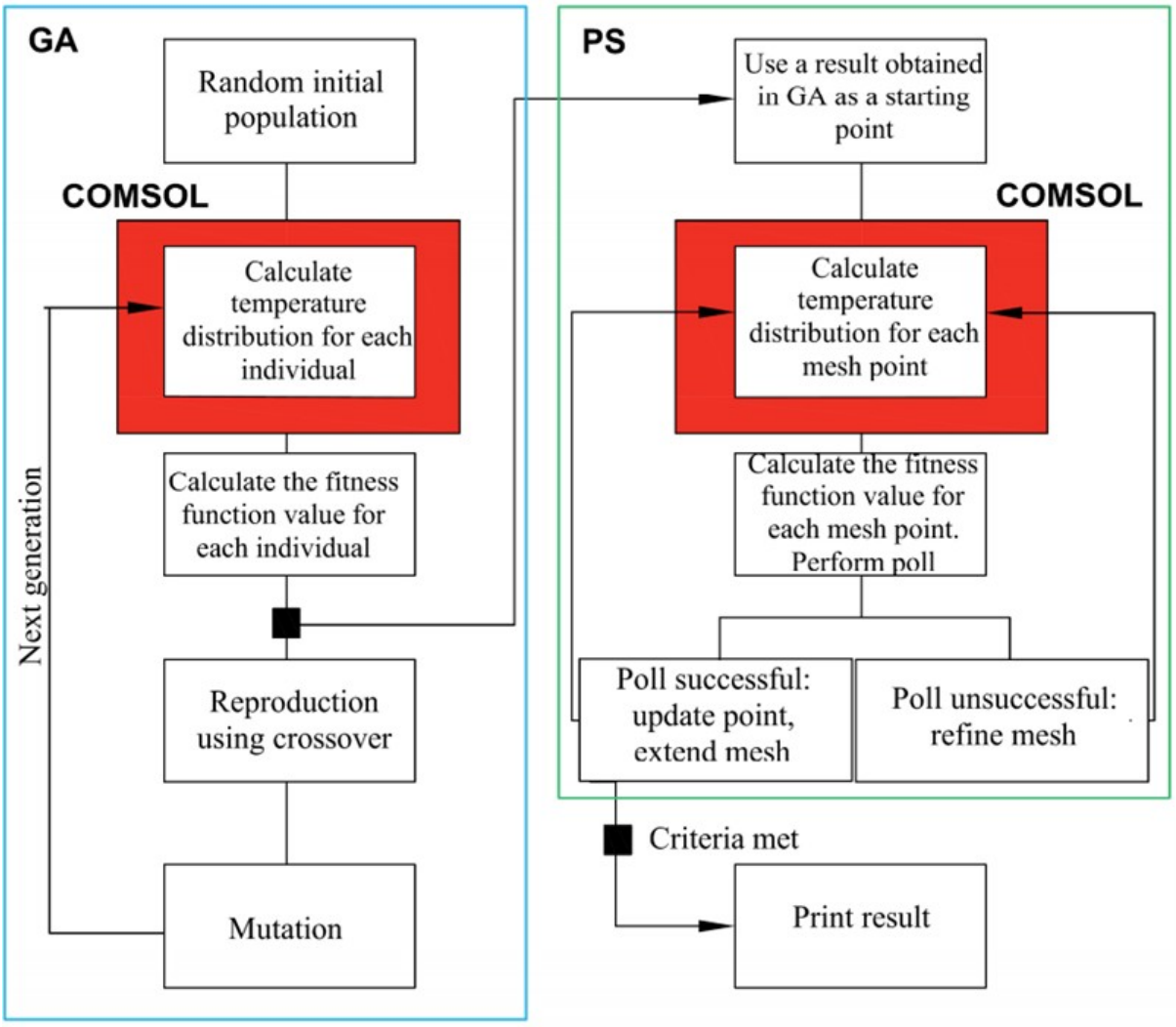

Figure 3.10: Workflow for solving inverse problem in active infrared thermography.

for human visual perception, human considers context and understands the whole situation also in a longer time perspective, this is a fundamental challenge in computer vision. Human understands that a cow dropped her head or arch her back because they she needs to reach food or avoid collision, the understanding of whether a cow is lame or not under adequate understanding of an entire scene is necessary but challenging.

The results of using edge detection is shown in Figure 3.19. When edges are extracted, the edges of the back can be segmented and its straightness calculated by comparing a straight line model.

3.2.2 Activity recognition

Figure 3.20 shows results for heat detection using a pre-trained convolution neural network model. A transfer learning technique is used. The pre-trained model is re-trained by using custom training images with labels. The pre-trained model is then used for detection of activity, in this case, mounting on another cow indicating on heat in unseen images.

3.2.3 Infrared thermography

Quantitative computational imaging such as by converting the observed sensor signal, in this case, it is the surface temperature fields to an unmeasured variable such as thermal conductivity fields. This is done via solving an inverse problem. The inverse problem is defined as a nonlinear least squares minimization problem, i.e., the $l2$ norm of difference between forward simulated data as to measured

Table 1: Evaluation of udder health using Infrared Thermography.

IRT camera	Breed/Species	Findings	Diagnosis	Reference
FLIRThermacam	Dairy cow	2.7°C change in udder surface temperature	Clinical mastitis	Scott *et al.*,2000
FLIRInframetrics 760	Holstein Friesian cow	1.02°C variation of udder surface temperature	Clinical Mastitis	Berry *et al.*,2003
FLIRInframetrics 760	Dairy cow	2.0°C increase of teat end temperature	Subclinical mastitis	Kunc *et al.*,2007
Thermal Cammera	Ayrshire and Holstein-Friesian	1 to 1.5°C increase in udder surface temperature	Clinical mastitis	Hovinen *et al.*,2008
IR Flex-Cam S,	Brown Swissand Holstein cows	0.9 to 1.5°C change in udder surface temperature	Subclinical mastitis	Colak *et al.*,2008
FLUKE TI 20™	Gir cows	change in udder surface temperature is 1.75-2.54°C	Subclinical mastitis	Porcionato *et al.*, 2009
FlexCam S	Brown Swiss	2.35°C change in udder surface temperature	Subclinical mastitis	Polat *et al.*,2010
FLIR System Serie-i	Sheep	change in udder surface temperature is 0.17 to 0.24°C	Subclinical and Clinical Mastitis	Martins *et al.*,2013
FLIR 760 IR Scanner	Dairy Cow	2.06°C differences in the surface temperatures of udder by E. coli infusion	Induced acute mastitis	Metzner *et al.*,2014
FLUKE Ti50FT Flexcam	Goat	4.92 °C temperature difference at teat end	Subclinical mastitis	Alejandro *et al.*,2014
FLIR TM	Holstein Friesian	Change of 2 to 3°C in udder surface temperature	Subclinical mastitis	Bortolami *et al.*, 2015
FLIR i5 camera	Holstein Friesian crossbred cows	0.72 to 1.05°C higher than healthy quarter.	Subclinical and Clinical mastitis	Sathiyabarathi *et al.*, 2016
FLIR T440	Holstein Frisian	Change of 1.35°C in udder surface temperature between positive and negative CMT scored quarter	Subclinical mastitis	Dogiovani *et al.*,2016

Figure 3.11: Summary of previous research on udder health monitoring using infrared thermography.

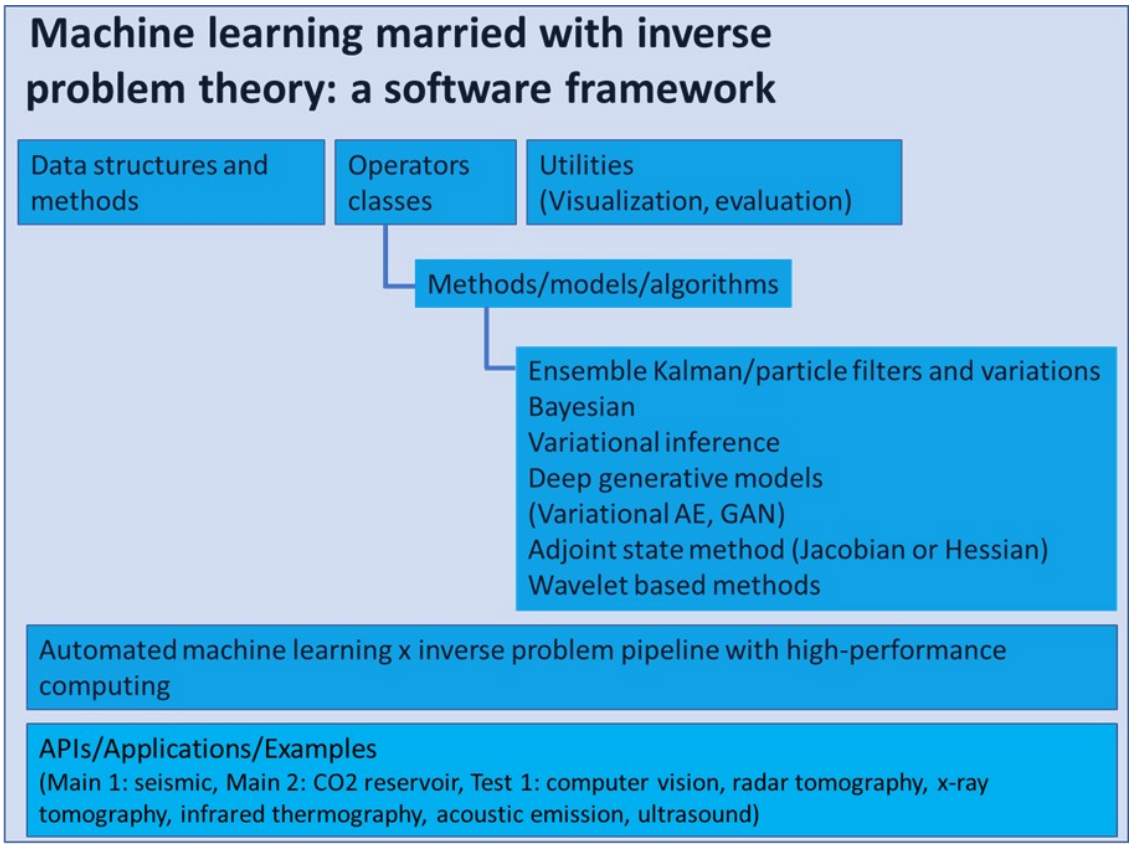

Figure 3.12: General framework for solving inverse problem using machine learning.

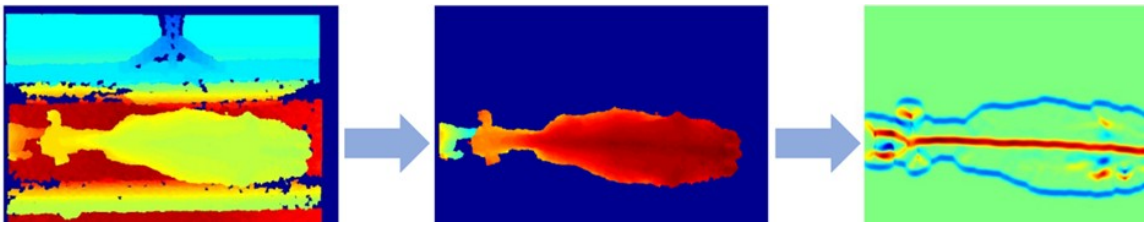

Figure 3.13: Lameness detection using RGBD imaging.

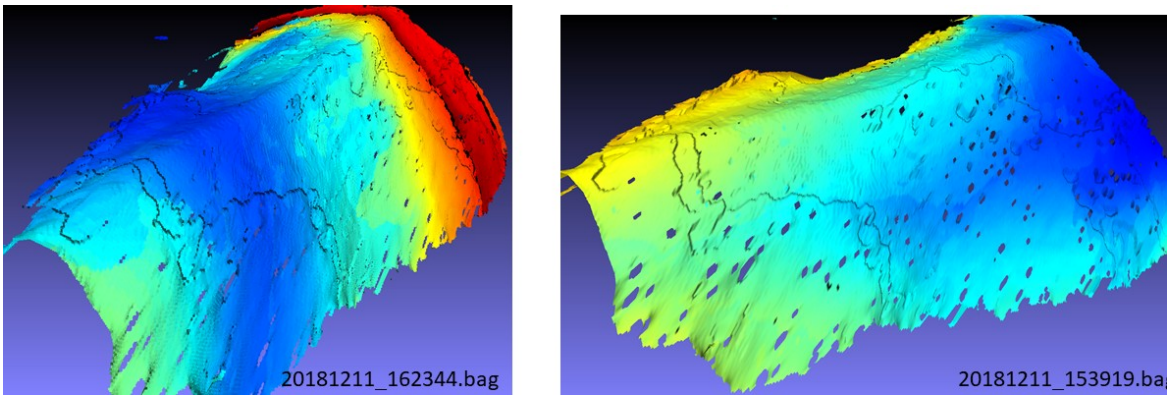

Figure 3.14: 3D model of cows no.1 and 2.

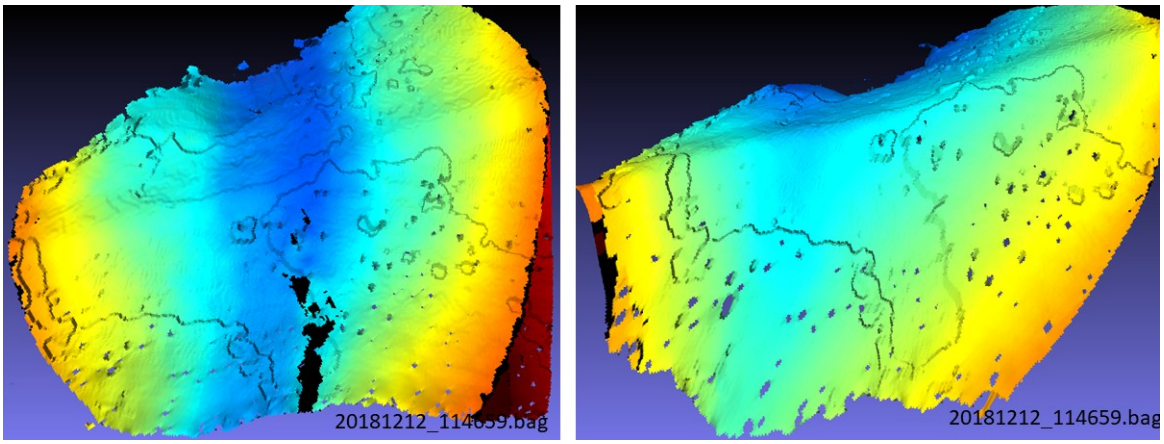

Figure 3.15: 3D model of cows no.3 and 4.

data. The forward simulated data are obtained by using the governing equation of the forward process with its parameters given by an initial guess. The optimization algorithms need to find the direction of updating to approach gradually.

Although in passive thermography setup, no active thermal source is applied. We adopt the assumption that the temperature distribution inside the udder satisfies the homogeneous linear heat equation [28].

$$\rho(\boldsymbol{x})c(\boldsymbol{x})\partial_t T(\boldsymbol{x},t)+\nabla\cdot(-\kappa(\boldsymbol{x})\nabla T(\boldsymbol{x},t))=0 \tag{3.1}$$

Figure 3.21 shows the mean temperature and standard deviation of udders of 23 cows. We see that individual differences exist both their mean temperature and in the homogeniety of distributions. Figures 3.22 and 3.23 shows that roughly the temperature fields can be separated as to their homogeneity. This is however considerably subjective and not quantitative.

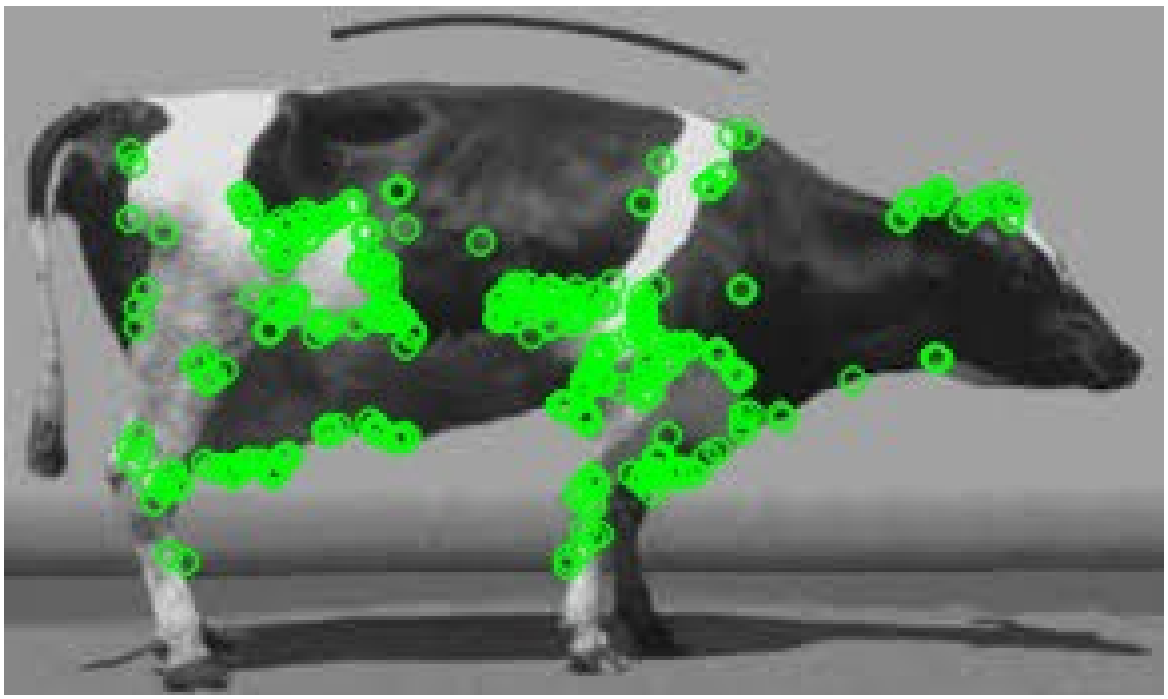

Figure 3.16: Keypoints via the ORB algorithms for lameness cow.

Figure 3.17: Keypoints via the ORB algorithms for healthy cow.

3.2.4 Artificial olfaction: GC-MS data and Cyranose

The sample preparation process and analysis procedure used for GC-MS analysis is described as below which is the same as Hettinga's work on the material and methods part. Ethanol which is a common VOC, was listed in Hettinga's Ph.D thesis but not in his article published on Journal of Dairy Science.

Compounds released from milk were collected on a train of traps filled with different solid sorbents to cover all components having a number of carbon atoms ranging from 4 to 15. They were analysed by GC-MS after thermal desorption of VOC from the collecting traps.

Figure 3.26 shows the VOC profiles of the 28 milk samples analyzed by GCMS. Only for reference purpose, Figure 3.28 shows results of the detection of odorants owing to fungi development in wood. What the result show is that no gas detected comparing to background, this is consistent with that the

Figure 3.18: Comparing keypoints detected of healthy and lameness cows.

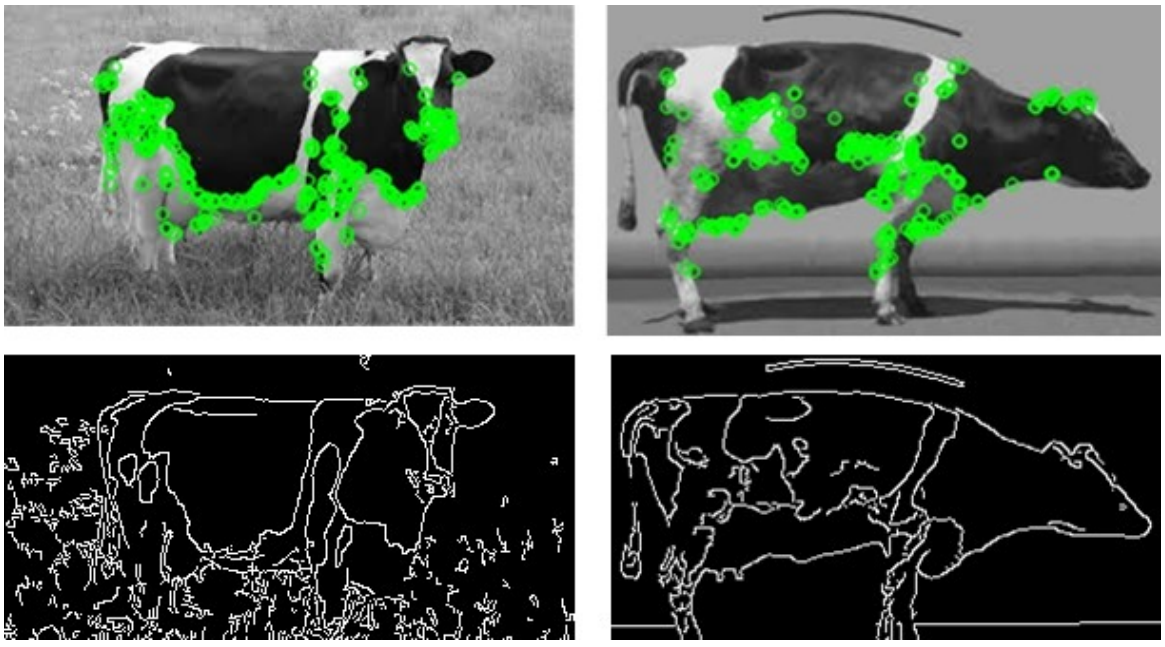

Figure 3.19: Comparing edges detected of healthy and lameness cows.

concentration of odorants giving the distinct smell of rot is much lower than the detection limit of the hyperspectral imaging Fourier transform infrared spectroscopy.

The following results are shared by Sensigent Inc. They are not produced within this project, but as references, the results are interesting and relevant. The Cyranose 320 was used to measure the headspace of three kefir products supplied by the customer. The customer requested a quick preliminary test to determine if the kefir products could be differentiated. Initial test results indicate each of the kefir samples can be distinguished from one another based on the headspace measurements. In a subsequent test, the Cyranose identified each kefir sample correctly when measured as an unknown. The identification accuracy was 100% with high statistical confidence. This shows the measurement protocol and results are robust and can be used for identification of the customer's kefir products. Follow up testing after 9 days refrigeration reveals the kefir products are well-discriminated from one

Figure 3.20: Activity detection using a pre-trained convolution neural network model

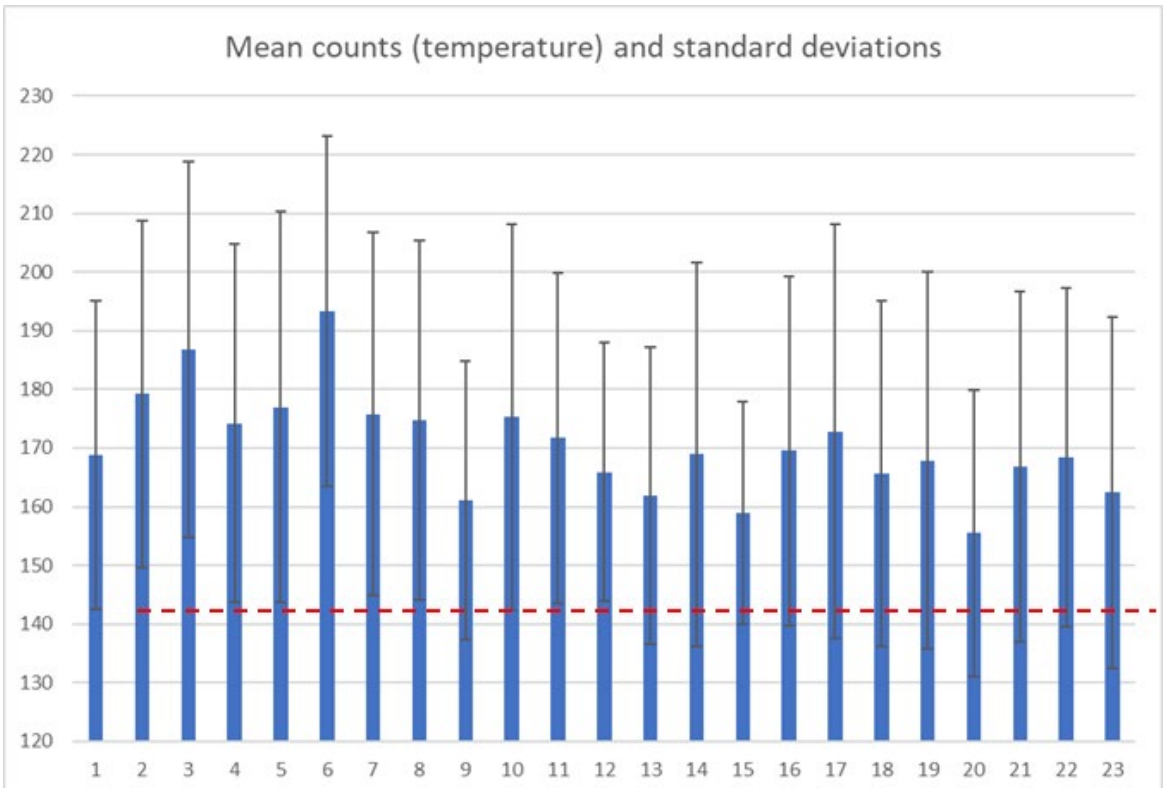

Figure 3.21: Mean and standard deviation in temperature of 23 cows

another. Aging produces dramatic changes in each of the products and the change is revealed along 3 new vectors (unique vector for each kefir) with principal direction along principle component 2. There is also greater intraclass variability in the aged products. Samples of the aged kefir products tested as unknowns are identified correctly as the aged product and not fresh.

Figure 3.29 illustrates headspace measurement set-up using Cyranose. Figure 3.30 shows the new unknown samples are represented by a star symbol with a label (1, 2 or 3) confirming the class identify of the sample tested. Figure 3.31 shows that the aged products are better discriminated from one another than the fresh products, and the variability (intraclass distance) is also greater. Age-related changes are identified along different vectors as projected onto 2-D plots, with most of the variance occurring along PC2 (now 25% of total). Once trained, the Cyranose was then used to identify new (unknown) aged kefir samples presented for measurement. In this case, neither the product class (BB kefir, Dvd Kefir, Zakvaska) or the age (fresh, aged) was known during the measurements. Each of the

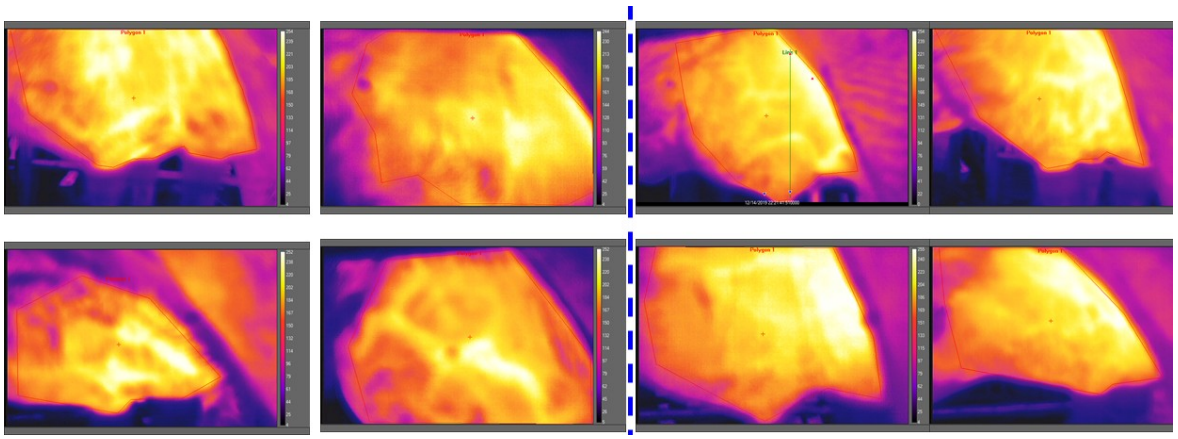

Figure 3.22: Infrared thermal images of cows showing homogeneous and non-homogeneous temperature fields

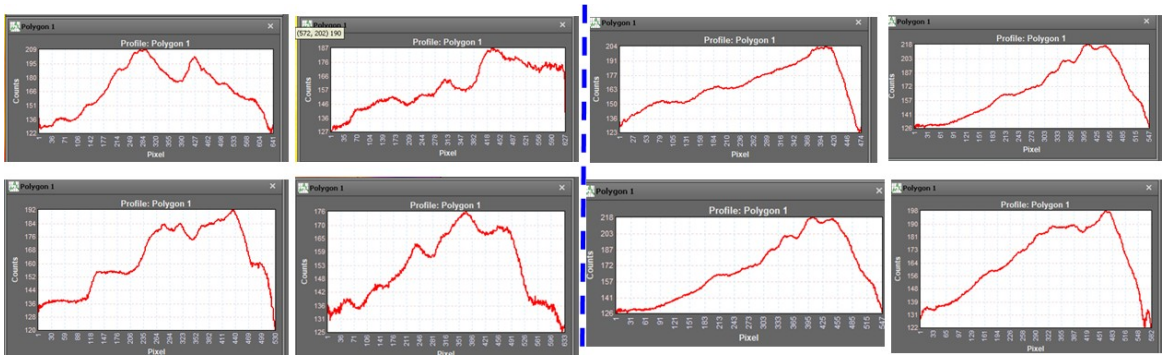

Figure 3.23: Temperature profile across the center of the udder in verticle direction.

Sample	M17	MRS	Blood Agar (A)	Blood Agar (AN)	VRBA	CRE	MRSA	ESBL	CowID	Quarter	Growth - Molde results
M1	6		93	145					2149	RF(HF)	Negative
M2	6		106	5					2149	LF(VF)	S. aureus (sparse growth)
M3	Overgrowth		Overgrowth			X	X		2149	RR(HB)	Negative
M4	8		118	33			X		2149	LR(VB)	S. aureus
M5			40	37			X		1518	RF(HF)	Negative
M6	23		187	320			X		1518	LF(VF)	CNS
M7			13	Overgrowth					1518	RR(HB)	Negative
M8			28	33					1518	LR(VB)	Mixed growth (contaminated?)
M9	28		350	12			X		1388	RF(HF)	S. aureus
M10	1		114	30			X		1388	LF(VF)	Negative
M11	268	115	311	Overgrowth		X	X		1388	RR(HB)	Mixed growth (contaminated?)
M12	18	7	205	128					1388	LR(VB)	Comybecterium bovis
M13	1		300	2					1225	RF(HF)	
M14	12	2	Overgrowth	66					1225	LF(VF)	
M15	Overgrowth	2	Overgrowth	Overgrowth	Overgrowth	X	X	X	1225	RR(HB)	
M16	7		237	18			X		1225	LR(VB)	
M17	11		192	10			X		1228	RF(HF)	Negative
M18	55		Overgrowth	98	Overgrowth		X		1228	LF(VF)	E. coli
M19			Overgrowth						1228	RR(HB)	Mixed growth (contaminated?)
M20	23	8	Overgrowth	30					1228	LR(VB)	Mixed growth (contaminated?)
M21	62		320	117			X		821	RF(HF)	Negative
M22	3		50	20			X		821	LF(VF)	Negative
M23	47	2	Overgrowth	124			X		821	RR(HB)	Negative
M24			19	2			X		821	LR(VB)	Negative
M25			7 (gruops of colonies)						2583	RF(HF)	Negative
M26	70		Overgrowth	279		X			2583	LF(VF)	CNS
M27	326		Overgrowth	300			X		2583	RR(HB)	CNS
M28	57		296	183			X		2583	LR(VB)	CNS

Counts of plates inoculatated
X = possible presence, it need

2149

Quarter	Growth - Molde results
RF(HF)	Negative
LF(VF)	S. aureus (sparse growth)
RR(HB)	Negative
LR(VB)	S. aureus

Figure 3.24: GCMS analysis samples.

samples tested was identified as belonging to the correct product class with a 5-star statistical rating (goodness of fit). Numerically, the probability estimate was very high (nearly 1.0 or 100%) and the intraclass distance was very low (mostly <3). The 3.2% Dvd kefir product exhibited great variation

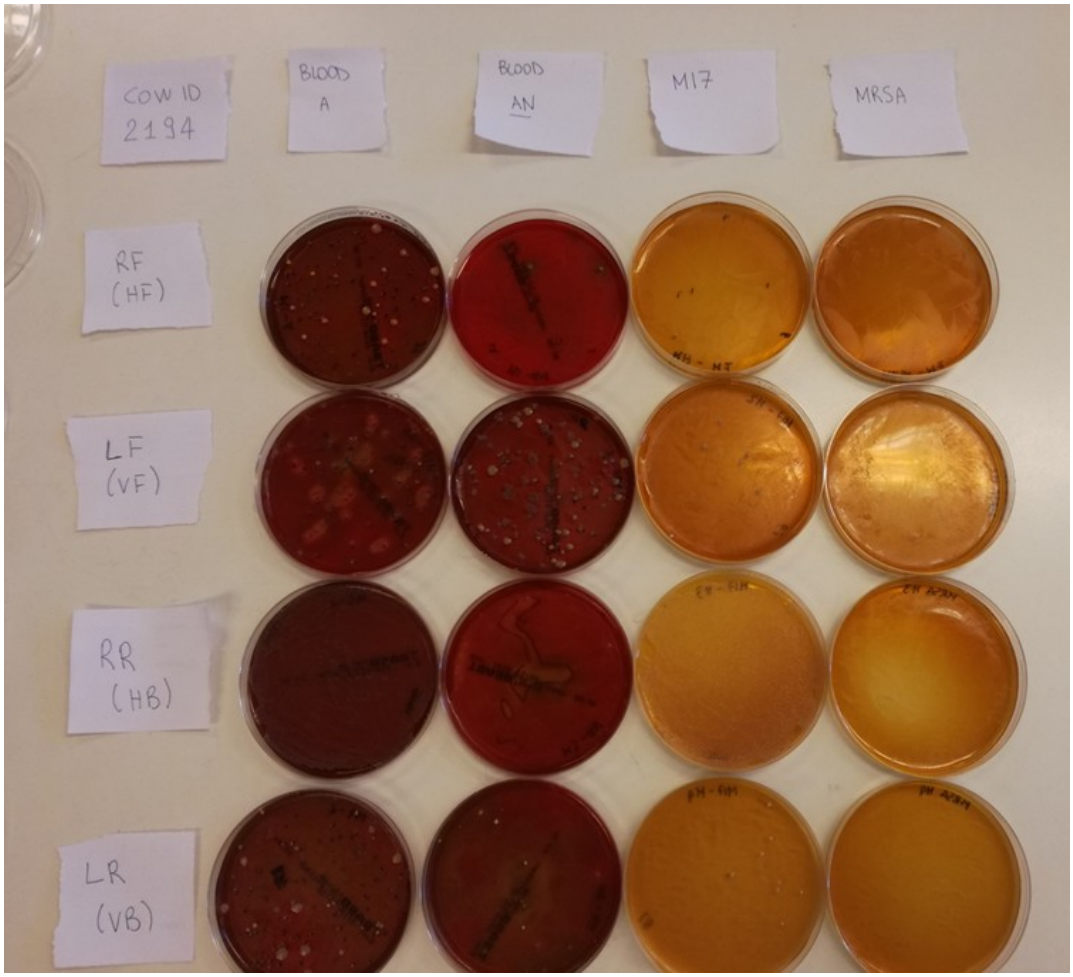

Figure 3.25: GCMS analysis sample images.

with aging than the other products. In Figure 2 the new unknown samples are represented by a star symbol with a label (1, 2 or 3) to identify the sample tested.

3.2.5 Visual-olfactory data fusion via graph convolution neural networks

Graph convolution neural networks provides a flexible architecture for dealing more complex inputs such as multi-modal data and spherical data. This is currently not studied much within the project.

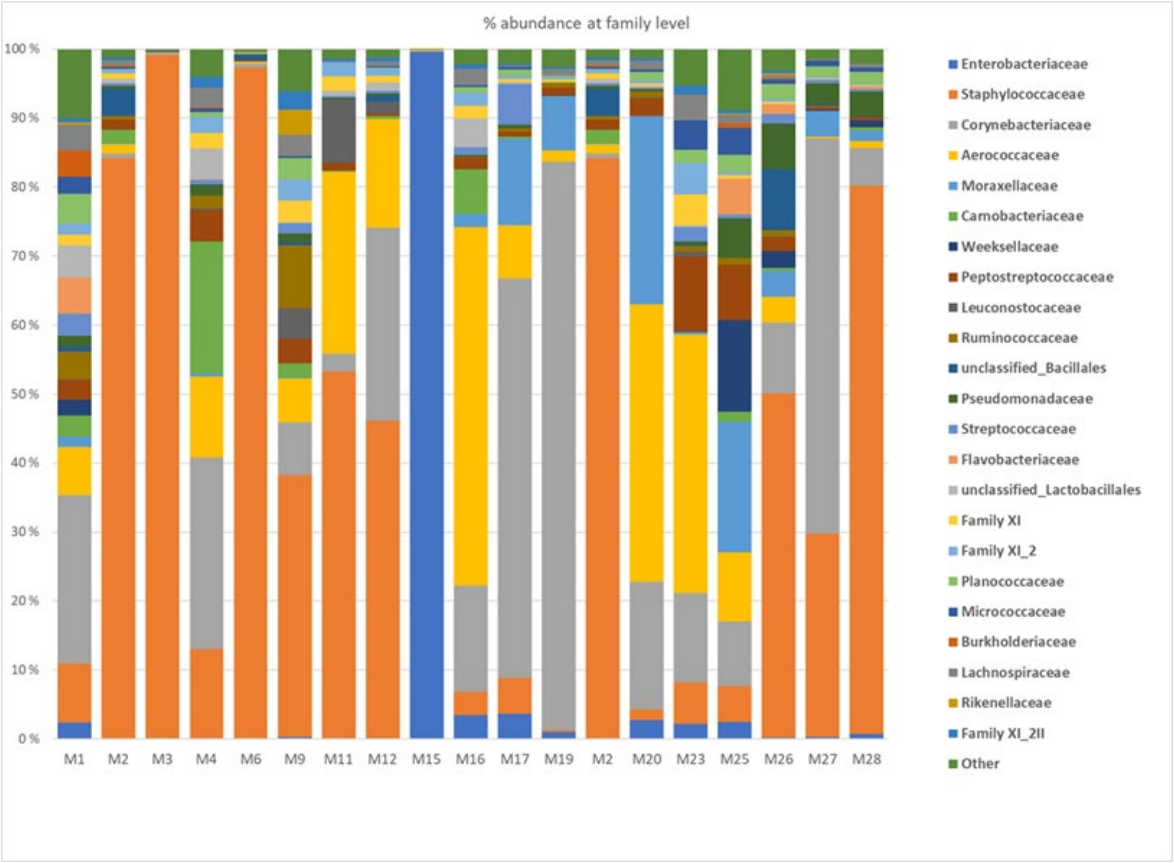

Figure 3.26: Heat map of VOC contents in the 28 samples being analyzed by GCMS.

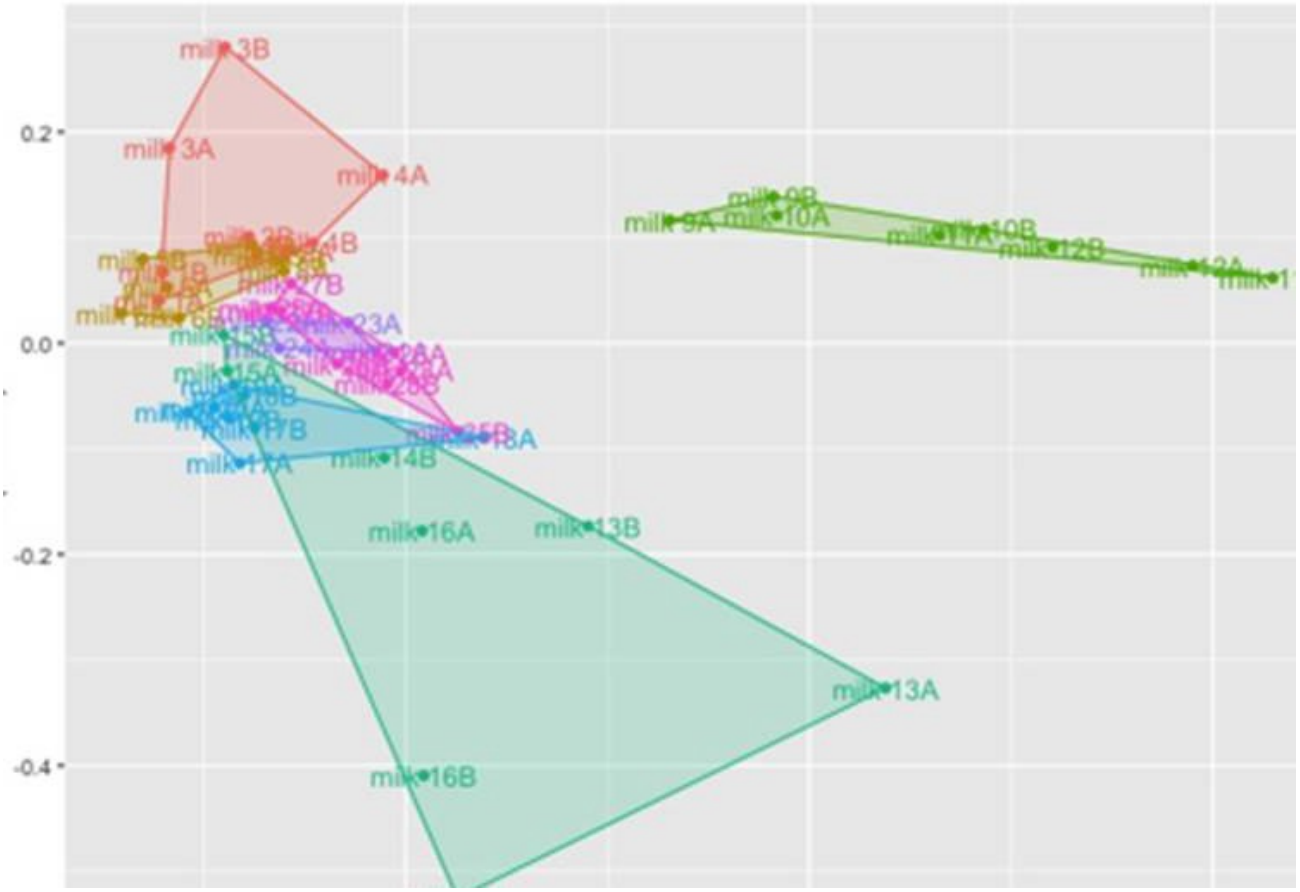

Figure 3.27: Principle component analysis av GCMS data.

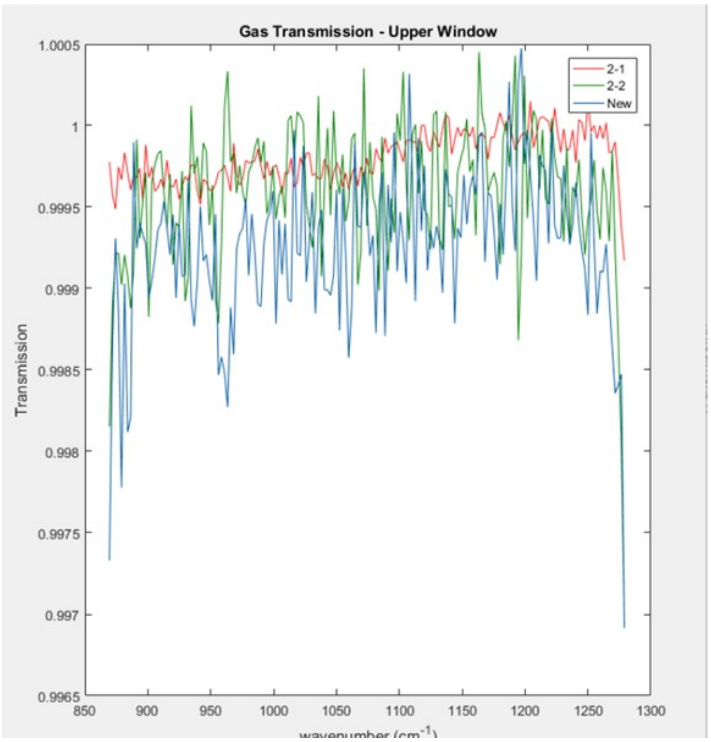

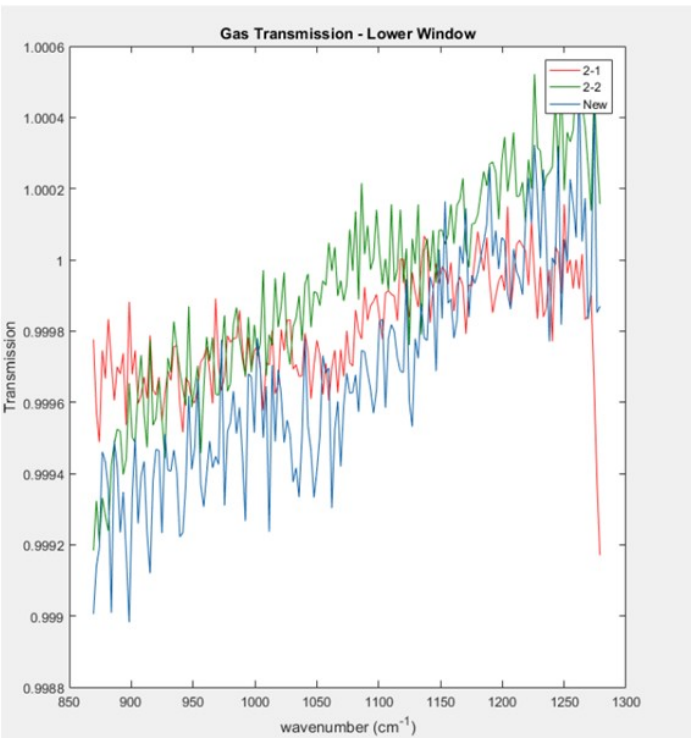

Figure 3.28: For reference only: detection of odorants via hyperspectral imaging FTIR.

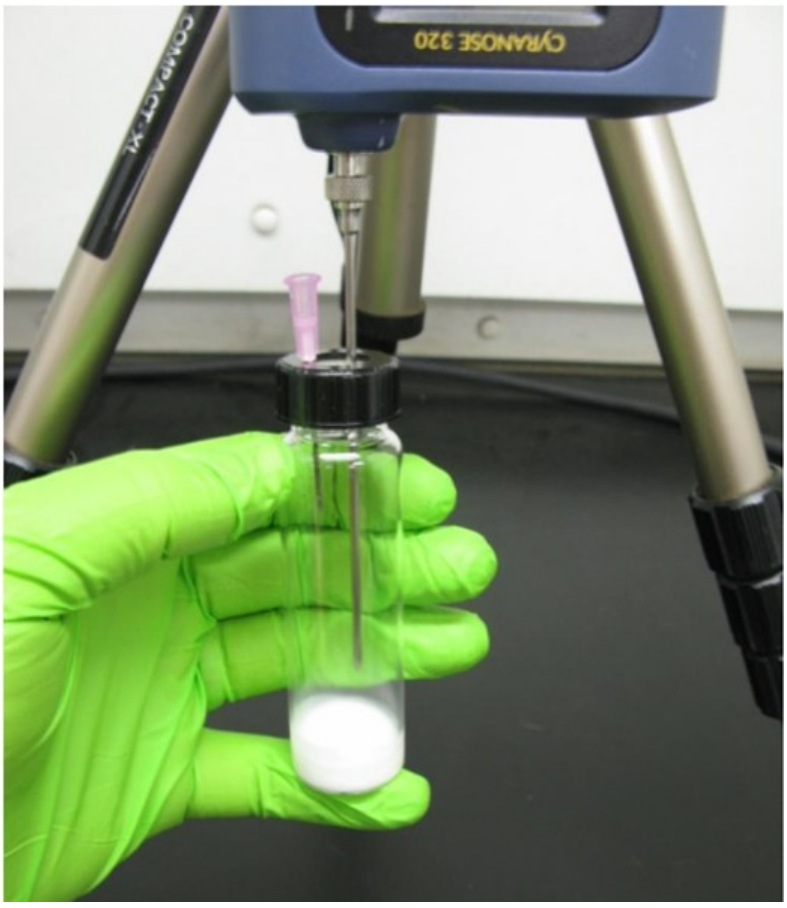

Figure 3.29: Headspace VOC measurement by Cyranose.

Method: DAN01	Test: What Kind of Product is the Sample?
Classes: 1: 25KEO – 2.5% BB Kefir 2: 253AK – 2.5% Zakvaska 3: 32KEO – 3.2% Dvd Kefir Setup: Vessels: 40ml Vials w Septum Sample Temp: 30 Celsius M_DistBetweenClass = 0 6.1310 6.4550 6.1310 0 11.6830 6.4550 11.6830 0 Cross Validation Percent Correct: 100%	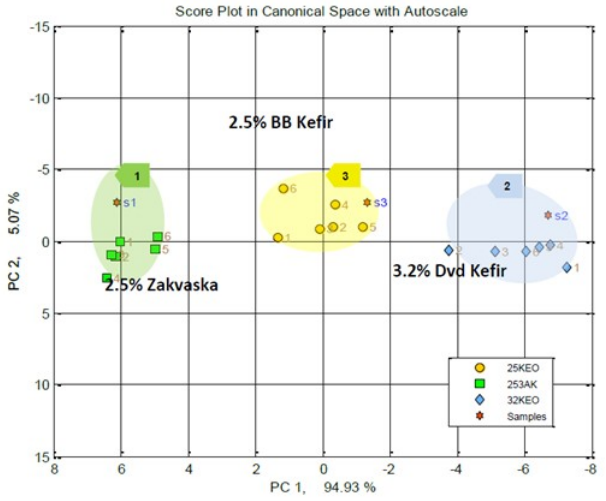
CDA_identification = Sample 1 belongs to class 2 , 253AK , (*****), CProb = 0.9216, MDist = 3.5089 Sample 2 belongs to class 3 , 32KEO , (*****), CProb = 1.0000, MDist = 2.7264 Sample 3 belongs to class 1 , 25KEO , (*****), CProb = 1.0000, MDist = 1.8425	

Figure 3.30: PCA for sample clustering with Cyranose data.

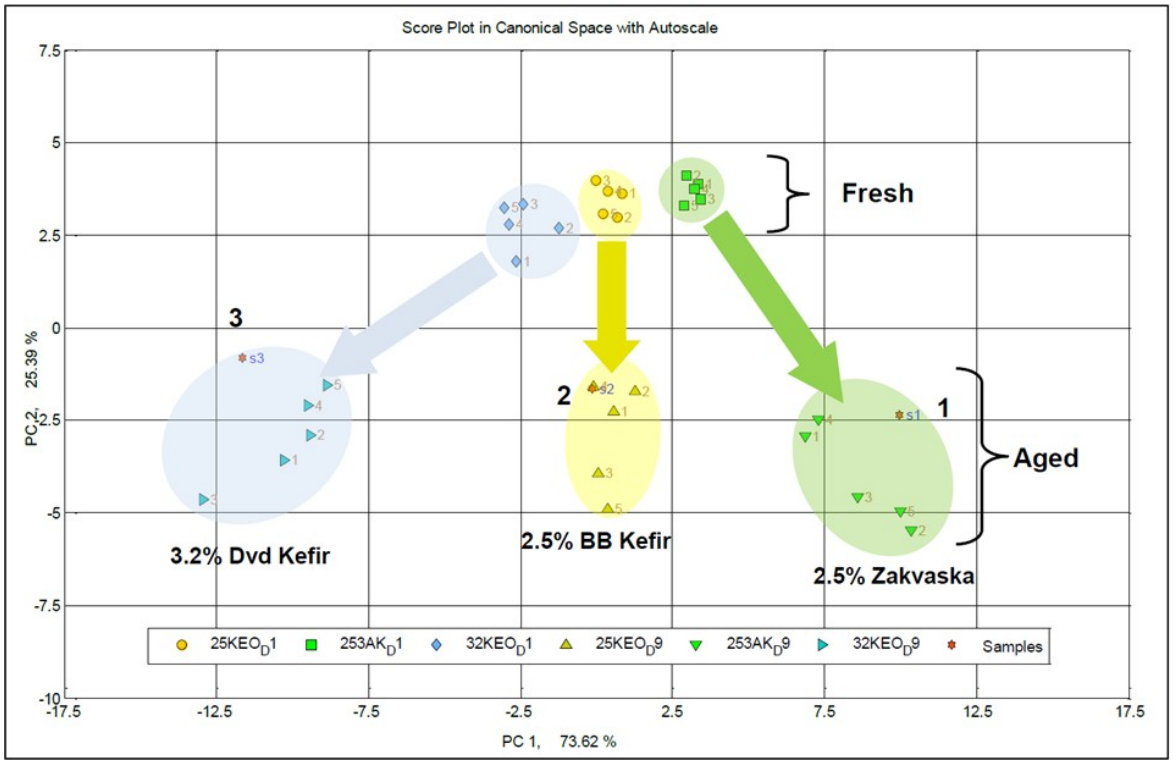

Figure 3.31: PCA for sample clustering with Cyranose data.

Chapter 4

Conclusion

We investigated detection of lameness via extraction of geometric features of arched back and dropped neck and head of cattle suffering pain. A commercial low-cost RGB-D imager (Intel Realsense D435) and its SDK (Software Development Kit) is used for **RGB-D imaging for 3D perception** while a cattle is standing in a milking robot. 3D models of cattle's back and neck are obtained via converting of point cloud to mesh in software meshlab. Within the limited sample set of cattles, although variations in arched angels in back and neck were found, no cattle showed signs of lameness, which was consistent with the ground truth. **Gait and behavior analysis** of these cattle in the panorama images and videos collected were hindered owing to that occlusions and that the activities of the animals are very limited (most of time they are standing or lying). Nevertheless, gait analysis - targeting imbalance and behavior (targeting estrus cycle detection) via deep convolution neural network models using open dataset was done. Our conclusion is that the combination of RGB-D perception, combined with gait and behavior analysis, health and welfare conditions including digital dermatitis and mastitis of cattle can be accurately assessed automatically with need of only few low-cost visual sensors for monitoring of multiple even a large amount of animals.

By using a **thermal imaging camera** (Flir tau2, spectral band: 7.5 13.5μm, sensitivity: $< 60mK$), the spatial and temporal variations in temperature of udder area of cattle while they are getting milked in milking robot were investigated. Within the limited sample set, obvious individual variations in mean temperatures and their standard deviations were shown. Ground truth of whether one of more of the cattle had mastitis infection was not accurately identified, it was with high-confidence from laboratory analysis that no cattle had mastitis during the data collection period. The conclusion is that passive infrared thermography definitely could provide useful data for extraction of information about the health of udders and cattle, harmlessly and low-costly (Only 1 sensor is needed). Variations in lighting condition owing to difference in shape and size of udder and their physical size and standing position were found to provide false input, which could be eliminated by simply not not using lighting during infrared thermal imaging. Activity of cow is considered to influence overall temperature but not their spatial distributions. Discrete Fourier transform and wavelet transform were used for image processing. Inversion algorithms for reconstructing images of udder for values of thermal conductivity and thermal capacity could provide a super-resolved image of mastitis infected area.

Artificial olfaction finds tremendous significant applications given adequate sensor for VOCs operating remotely or in the ambient without the need for guiding gas through a chamber such for tunable diode laser absorption spectroscopy. The sensing of odorants using a traditional laboratory **gas chromatography - mass spectroscopy** of 24 milk samples (15 infected and 9 healthy controls) for the purpose of identifying volatile organic compounds (VOC) biomarker for mastitis infected milk were not successful. The reason being that unknown bacteria developed during the storage and transport of the samples contributed from dairy farms complicated the samples. Whilst, a doctoral research carried out in a university in the Netherlands showed that ethanol is a distinct biomarker for mastitis. Indeed, the discovery of a reliable biomarker in itself a research topic which is out of the scope of this project. A trial of using hyperspectral Fourier transform infrared spectroscopy for the detection of odorants conducted by us failed to detect any gas owing to that the concentration of odorants could

be order or magnitude lower than ppm range. Such low concentrations need MOS chemoresistive gas sensors, especially those emerging sensing elements made of nanowire, nanotubes and graphene for their higher sensitivity. A **photo ionization detector (PID)** type gas sensor calibrated for the detection of ethanol at ppm range is tested in laboratory where the PID sensor is exposed to the head space of mastitis infected milk and healthy controls.

We have evaluated **Hyperspectral imaging (short wavelength infrared and visual near infrared)**analysis of milk in powder form after removing water for detection of mastitis causing pathogens such as Escherichia coli (E. coli), Streptococcus uberis and Staphylococcus aureus. A **bioradar** sensor for respiratory pattern monitoring is also considered to provide useful information. These cannot be conducted within this project.

The scope of this research is limited to feasibility studies such that the size and quality of dataset generated is considerably limited so as for the signal processing and machine learning algorithms. Results obtained in this pre-project with very limited scope show that visual and olfactory sensory perception could provide necessary and sufficient information about health and welfare condition of animals at a low cost and ambient sensing manner without need for animals to carry a sensor each. Early-stage mastitis infected cattle can be detected by collaboratively fusion of data from gait and behavior analysis, infrared thermography imaging, and detection of mastitis biomerkers. Early-stage digital dermatitis infected cattle can be detected via fusion of data from RGBD perception, gait and behavior analysis. Hyperspectral imaging and bioradar provides additional useful data.

Chapter 5

Future work

Figure 5.1 shows a nanosensory array based on MOS nanowires, carbon nanotubes and graphene for high-sensitively and high-selectively detection of VOCs. The nanoarray generates a large dataset, which is obtained using a sample size of 100 clinical tests and continuous data streaming with a sampling rate of 100 Hz per analysis. Nanosensor responses over the entire analysis period (usually seconds to few minutes) will be recorded using sampling frequency of 100 Hz such that both the temporal and dynamic properties of the interaction between sensor and analytes are recorded to provide robust features for clustering and classification of odours. Our idea is to develop a 10 x 10 (100 pixel) nanosensor array and interface circuit integrated with CMOS compatible fabrication for high-dimensional and robust sensing; this is shown in Figure 1. It enables standardized nanosensor array chips for compatibility with other electronics and communication protocols. The 10 x 10 nanosensor array is made of metal oxide nanowire (such as tin oxide (SnO2), zinc oxide (ZnO), copper oxide (CuO)), graphene and carbon nanotubes as sensing elements. Their sensing characteristics are controlled by doping with various metal nanoparticles, applying organic functional compounds, and utilizing temperature modulation. New DNN models and algorithms will be developed; this is shown in Figure 2. This development needs to develop a method to encode the sensor responses patterns into image data format suitable for further adaptation of established DNN models and algorithms. Another method is based on encoding of the sensor response patterns into time-series waveform data, then adopting methods used for speech recognition. We believe that either existing DNN models and algorithms can generate interesting results, or else new DNN models and algorithms can be inspired by mimicking the olfactory intelligence.

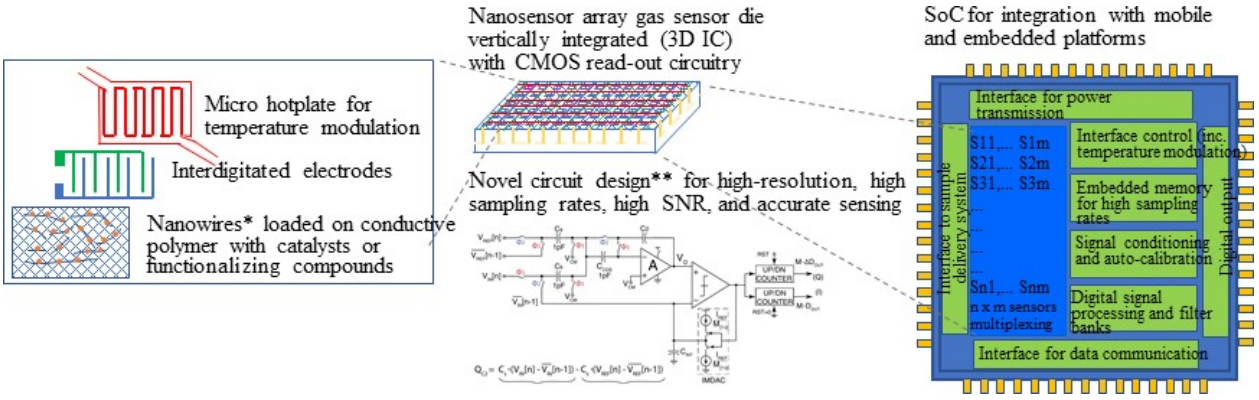

Figure 5.1: Nanosensor array for high-sensitively and high-selectively detection of VOCs.

Figure 5.2 shows the neuro-information processing system for knowledge discovery based on multilayer deep artificial neurual networks and encoding-decoding system.

Our ambition in digitalized agriculture and aquaculture calls for robust sensory technologies for uncovering knowledge in biological systems with focus on diseases and stress detection, feeding

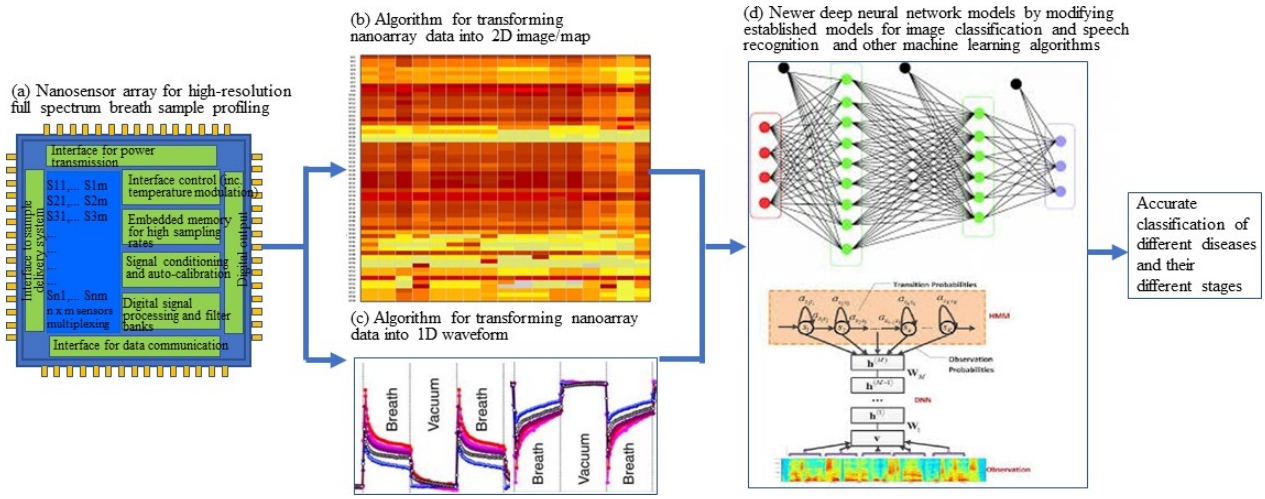

Figure 5.2: Neuro-information processing system for olfactory knowledge discovery.

monitoring and phenotyping. We think hyperspectral imaging and artificial olfactory excellently fulfils these requirements, because they provide quantitative chemical information in a high-dimensional feature space, which under known temperature and pressure, represents a complete knowledge of the biological system. Hyperspectral cameras catch reflected electromagnetic radiations characteristic to different materials in hundreds of contiguous bands, thus provides 2D mapping of chemicals and their abundances. Unique to biological systems, volatile organic compounds (VOCs), which are often emitted as results of metabolism of pathogens, carry important signatures of diseases. Highly sensitive olfaction systems such as dogs' nose and insects' antenna, possible also electronic nose made of highly sensitive MOS nano-sensors and tuneable diode laser absorption spectroscopy (TDLAS), as well as hyperspectral imaging cameras at the long wave infrared region (LWIR), can capture VOC information over a long distance (hundreds of meters). Furthermore, we think, by exploring the collaborative interaction of visual and olfactory perception as inspired by neurocognitive research findings , a new paradigm of artificial intelligence and machine learning could be generated in this project. This new paradigm may be an extension of Markov random field model, automatic kernel selection-based support vector machine, and brain-inspired intelligence models. When connecting the state-of-the-art technologies in hyperspectral imaging and olfactory sensing to digitalized agriculture, for example, for disease detection, we found there remain many tough challenges (in both performances and costs of both hardware and software). We believe the right pathway is to utilize hyperspectral cameras and olfaction sensory of dogs or insects combined with an electronic nose to identify biological system-invariant features, which can be adequately captured by fewer sensors and bands for a specific problem, leading to simple and low-cost but intelligent sensory system. To do this, we need a visual-olfactory multi-modal dataset and a robust learning algorithm making use of multi-sensory information collaboratively. Thus, this project develops new multimodal sensory and computational methodologies for diseases detection using visual-olfaction bimodal sensing. A large high-dimensional dataset is generated using simultaneously hyperspectral imaging cameras and electronic noses for two severe and representative diseases, i.e., mastitis in dairy cattle and moth in crops . Figure 1 illustrations the specific problem cases, the new sensory methodologies, and our initiative in establishing a new open dataset for promoting artificial intelligence research. We strive to develop computational methods that learn in hyperspectral imaging data and olfactory data in a collaborative manner for higher accuracy and speed in classification tasks suffering from curse of dimensionality. This is inspired by neurocognitive studies in visual- olfactory cross-modal integration in human. We will be focusing on abstracting underlying the physical, statistical, mathematical, geometrical (projection) and neurocognitive principles such as to adaptively build new models upon the state-of-the-art ones. Performance in mastitis and moth detection of our methods are compared to baseline methods such as support vector machine, discriminative analysis, and principle component analysis. Figure 2 depicts the computational methodologies we are focusing

on, and some of the state-of-the-art methods we will use as baseline methods for comparison.

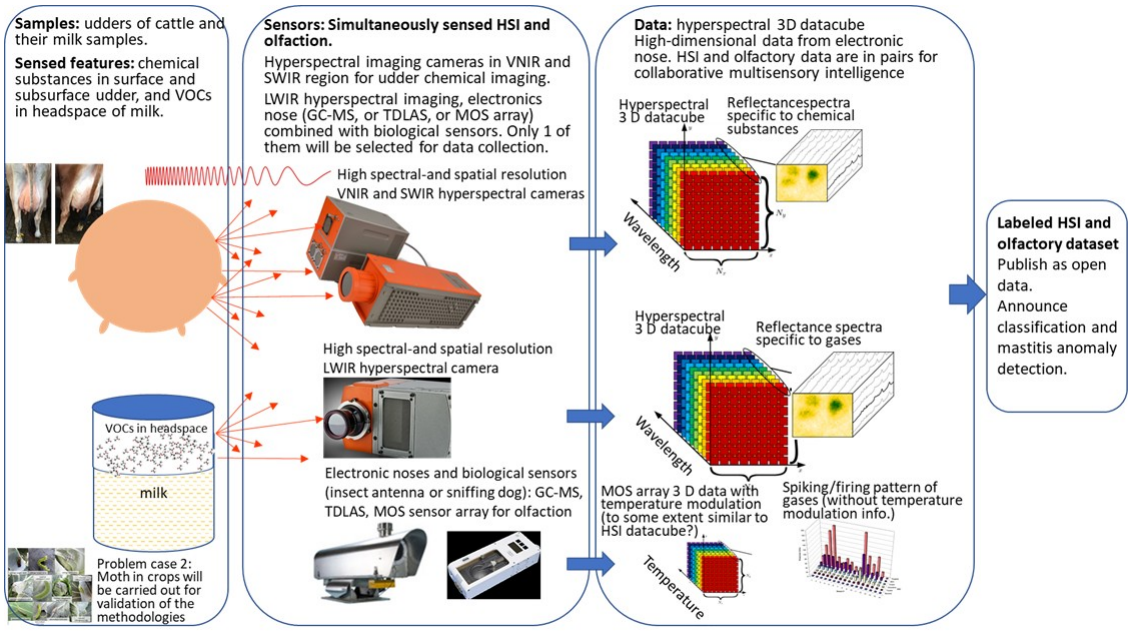

Figure 5.3: Illustrations of the specific problem cases, the new sensory methodologies, and our initiative in establishing a new open dataset for promoting artificial intelligence research.

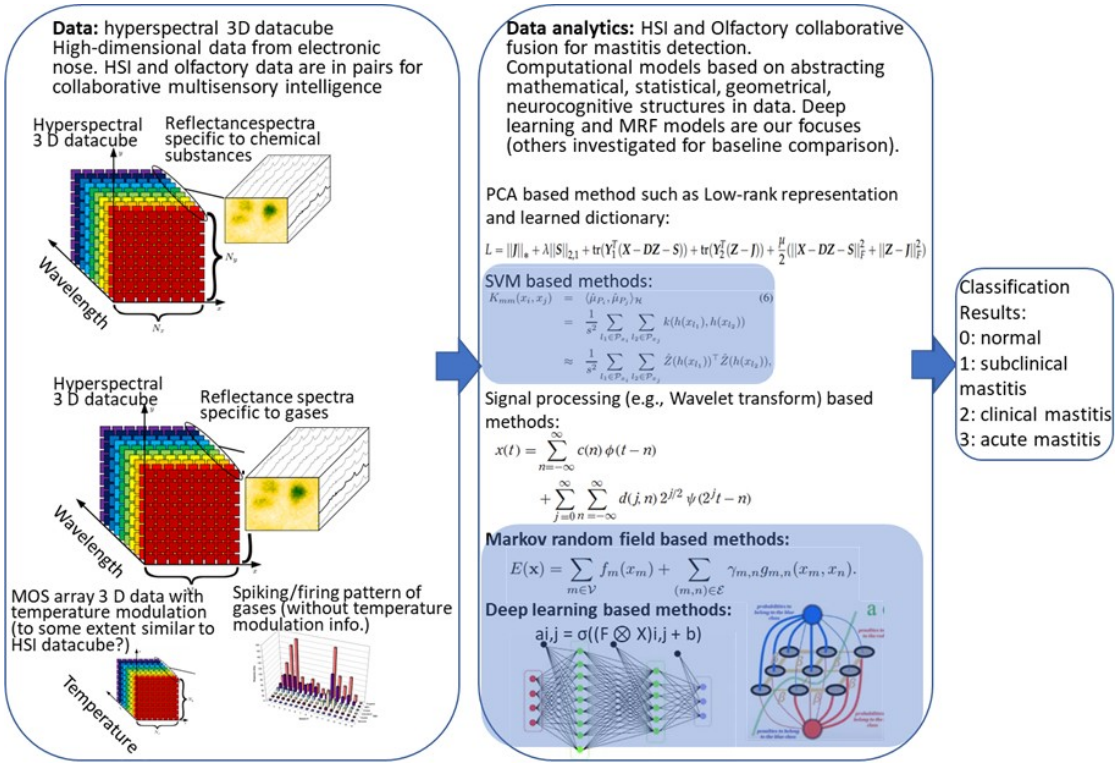

Figure 5.4: Computational methodologies we are focusing on, and some of the state-of-the-art methods we will use as baseline methods for comparison.

Figure 5.5 shows the results of a neuromorphic chip for hardware realization of neural computing using electronic nose data [26].

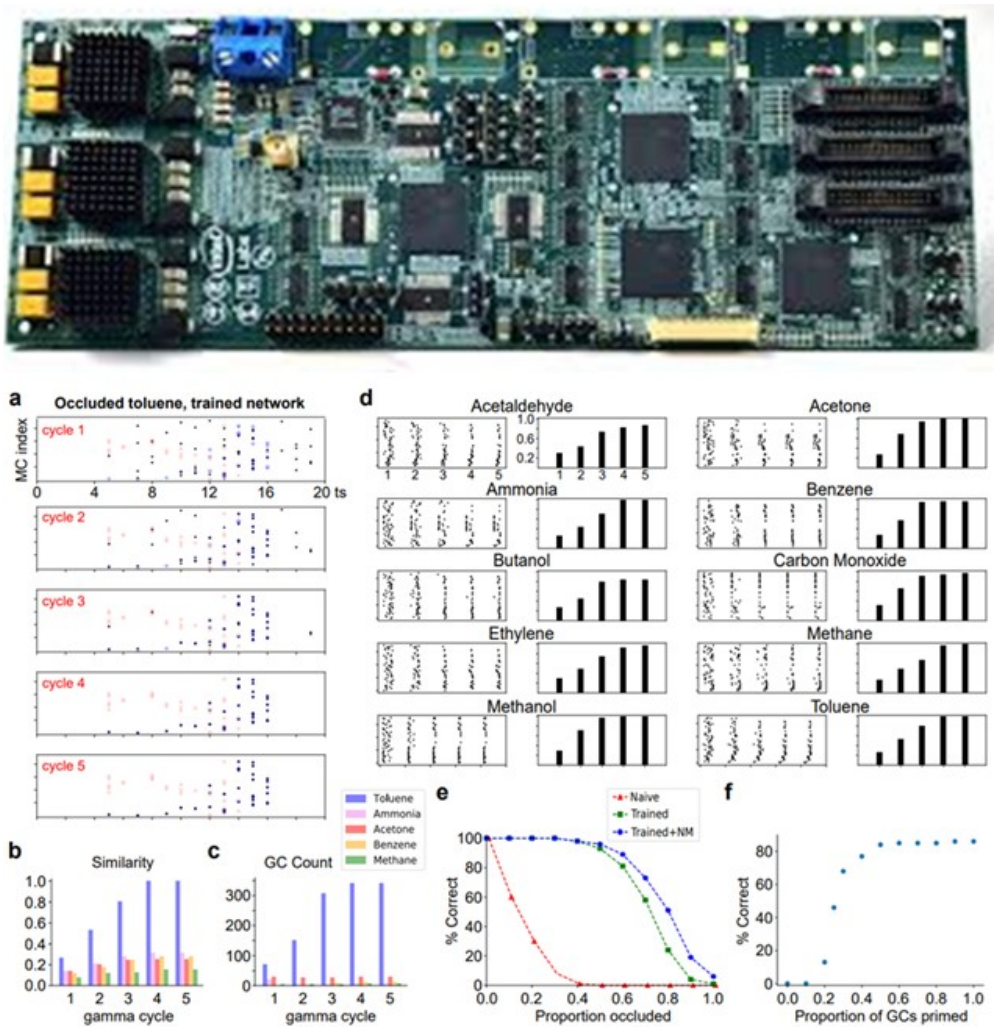

Figure 5.5: Future in-process real-time processing using neuromorphic chips.

Bibliography

[1] Tony Lin, Hongbin Zha, and Sang Uk Lee. "Riemannian manifold learning for nonlinear di- mensionality reduction". In: *European Conference on Computer Vision*. Springer. 2006, pp. 44– 55.

[2] Anders Brun. "Manifolds in image science and visualization". PhD thesis. Institutionen för medicinsk teknik, 2007.

[3] KA Hettinga et al. "Detection of mastitis pathogens by analysis of volatile bacterial metabolites". In: *Journal of Dairy Science* 91.10 (2008), pp. 3834–3839.

[4] KA Hettinga et al. "The influence of incubation on the formation of volatile bacterial metabolites in mastitis milk". In: *Journal of dairy science* 92.10 (2009), pp. 4901–4905.

[5] KA Hettinga et al. "The origin of the volatile metabolites found in mastitis milk". In: *Veterinary microbiology* 137.3-4 (2009), pp. 384–387.

[6] Kaspar Arthur Hettinga. *Quality control of raw cows' milk by headspace analysis: a new approach to mastitis diagnosis*. 2009.

[7] Gang Peng et al. "Diagnosing lung cancer in exhaled breath using gold nanoparticles". In: *Nature nanotechnology* 4.10 (2009), pp. 669–673.

[8] Caroline Viguier et al. "Mastitis detection: current trends and future perspectives". In: *Trends in biotechnology* 27.8 (2009), pp. 486–493.

[9] Dominique Perrault-Joncas and Marina Meila. "Metric learning and manifolds: Preserving the intrinsic geometry". In: *Preprint Department of Statistics, University of Washington* (2012).

[10] Kasper A Hettinga, Frank AM de Bok, and Theo JGM Lam. "Practical issues in implementing volatile metabolite analysis for identifying mastitis pathogens". In: *Journal of dairy science* 98.11 (2015), pp. 7906–7910.

[11] Jonathan Huang et al. "Speed/accuracy trade-offs for modern convolutional object detectors". In: *Proceedings of the IEEE conference on computer vision and pattern recognition*. 2017, pp. 7310– 7311.

[12] Morad K Nakhleh et al. "Diagnosis and classification of 17 diseases from 1404 subjects via pattern analysis of exhaled molecules". In: *ACS nano* 11.1 (2017), pp. 112–125.

[13] Pamela L Ruegg. "A 100-Year Review: Mastitis detection, management, and prevention". In: *Journal of dairy science* 100.12 (2017), pp. 10381–10397.

[14] Yu-Chuan Su and Kristen Grauman. "Learning spherical convolution for fast features from 360 imagery". In: *Advances in Neural Information Processing Systems*. 2017, pp. 529–539.

[15] Xiaomin Xi et al. "Ultra-performance liquid chromatography-quadrupole-time of flight mass spectrometry MSE-based untargeted milk metabolomics in dairy cows with subclinical or clinical mastitis". In: *Journal of Dairy Science* 100.6 (2017), pp. 4884–4896.

[16] Taco S Cohen et al. "Spherical cnns". In: *arXiv preprint arXiv:1801.10130* (2018).

[17] Benjamin Coors, Alexandru Paul Condurache, and Andreas Geiger. "Spherenet: Learning spherical representations for detection and classification in omnidirectional images". In: *Proceedings of the European Conference on Computer Vision (ECCV)*. 2018, pp. 518–533.

[18] Carlos Esteves et al. “Learning so (3) equivariant representations with spherical cnns”. In: *Proceedings of the European Conference on Computer Vision (ECCV)*. 2018, pp. 52–68.

[19] Muhammad Asad Lodhi and Waheed U Bajwa. “Detection theory for union of subspaces”. In: *IEEE Transactions on Signal Processing* 66.24 (2018), pp. 6347–6362.

[20] Mathias Trabs. “Bayesian inverse problems with unknown operators”. In: *Inverse Problems* 34.8 (2018), p. 085001.

[21] Michaël Defferrard et al. “DeepSphere: a graph-based spherical CNN”. In: *International Confer- ence on Learning Representations*. 2019.

[22] Nathanaël Perraudin et al. “DeepSphere: Efficient spherical convolutional neural network with HEALPix sampling for cosmological applications”. In: *Astronomy and Computing* 27 (2019), pp. 130–146.

[23] Kuan-Hsun Wang and Shang-Hong Lai. “Object Detection in Curved Space for 360-Degree Camera”. In: *ICASSP 2019-2019 IEEE International Conference on Acoustics, Speech and Signal Processing (ICASSP)*. IEEE. 2019, pp. 3642–3646.

[24] Dawen Yu and Shunping Ji. “Grid based spherical cnn for object detection from panoramic images”. In: *Sensors* 19.11 (2019), p. 2622.

[25] Shih-Han Chou et al. “360-Indoor: Towards Learning Real-World Objects in 360deg Indoor Equirectangular Images”. In: *The IEEE Winter Conference on Applications of Computer Vision*. 2020, pp. 845–853.

[26] Nabil Imam and Thomas A Cleland. “Rapid online learning and robust recall in a neuromorphic olfactory circuit”. In: *Nature Machine Intelligence* 2.3 (2020), pp. 181–191.

[27] Yeonkun Lee et al. “SpherePHD: Applying CNNs on 360° Images with Non-Euclidean Spher- ical PolyHeDron Representation”. In: *IEEE Transactions on Pattern Analysis and Machine Intelligence* (2020).

[28] Manuel Pena and María-Luisa Rapún. “Application of the topological derivative to post-processing infrared time-harmonic thermograms for defect detection”. In: *Journal of Mathematics in Industry* 10.1 (2020), p. 4.

[29] Qin Yang et al. “Rotation Equivariant Graph Convolutional Network for Spherical Image Classification”. In: *Proceedings of the IEEE/CVF Conference on Computer Vision and Pattern Recognition*. 2020, pp. 4303–4312.

[30] Pengyu Zhao et al. “Spherical Criteria for Fast and Accurate 360° Object Detection.” In: *AAAI*. 2020, pp. 12959–12966.